UiT
THE ARCTIC
UNIVERSITY
OF NORWAY

Department of Physics and Technology

Filament motions in magnetized plasmas

Mikhail Enikeev

FYS-3900 Master's thesis in physics 60 SP, February 2018

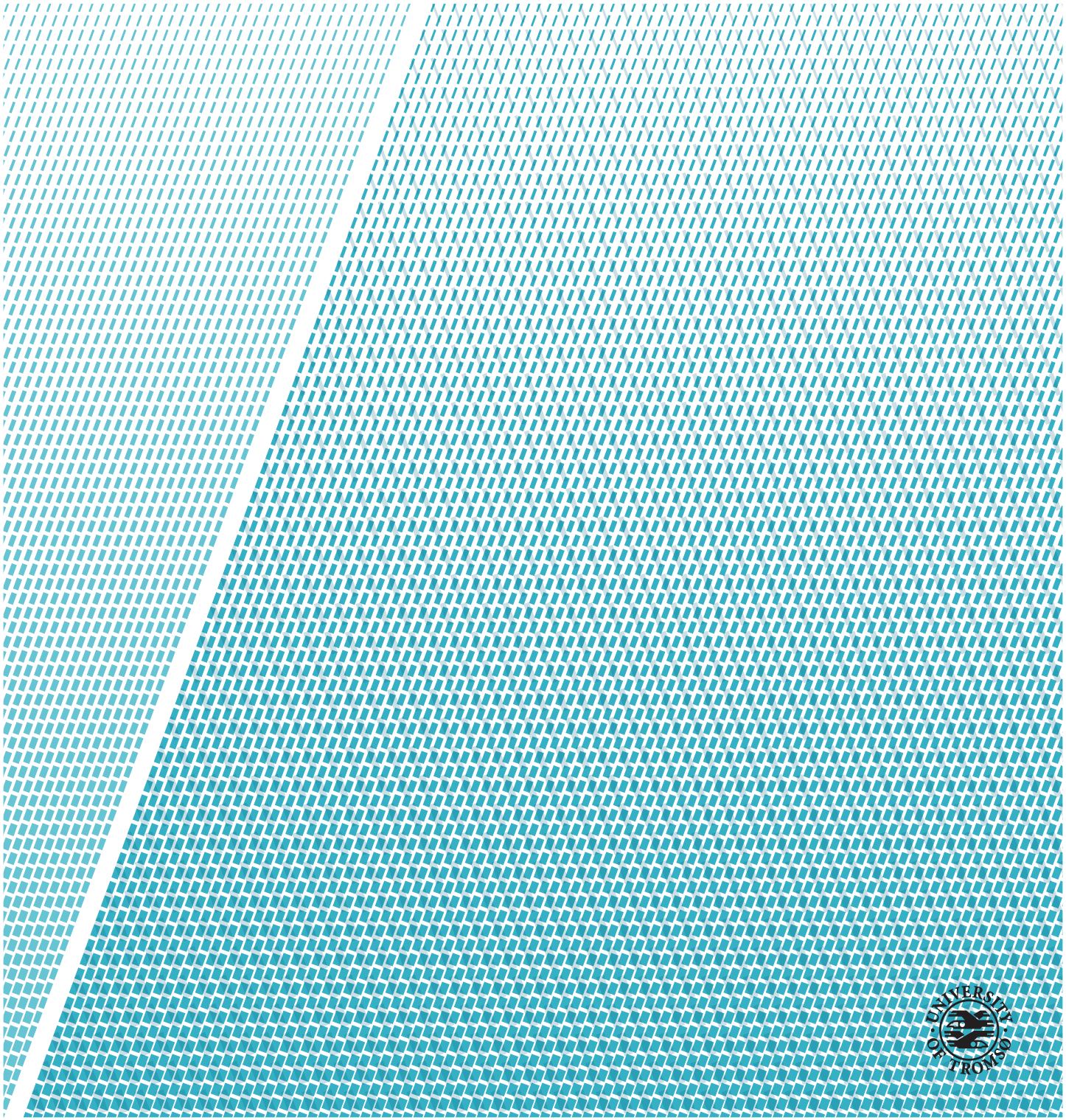

“Physics is really nothing more than a search for ultimate simplicity, but so far all we have is a kind of elegant messiness”
– Bill Bryson

“Bruk fornuften!”
–Einar Mjølhus

Acknowledgements

All good and bad things always come to the end, and now I am almost done with my studies.

Fisrt of all, I would like to thank Troms fylkeskommune, the administration of the Russian-Norwegian school, Murmansk Arctic State University and Statens Lånekassen for providing me an unique possibility to study in Norway.

I want to say big thank to my supervisors Ralph Kube and Odd Erik Garcia for showing me how complicated and at the same moment interesting plasma physics really is and for very attentive and professional supervision. And I would specially thank Ralph for his composure and all the consultations that he provided to me, especially about obvious and very stupid things.

I would also like to thank everyone who has been following me during this amazing student journey, including friends, students at the university, UiT's staff and my employers.

I would also like to thank Erlend Graff and other contributors, whose LaTeX-template I have used. It has really allowed me to concentrate on writing and forget about formating issues.

I thank my family for the constant support and keeping me motivated all the time.

And of course, my last but not least acknowledgement goes to TS. I would never do it without your support.

Abstract

Interchange motions of magnetized plasmas due to either a non-uniform magnetic field or a gravitational field lead to charge polarization within a filamentary structure and set up convection. In this project we have provided a clear derivation of the two-field model equations that describe these filament motions. We have also derived an energy theorem for small amplitude oscillations.

We have derived the electron temperature equation for interchange motions and also described the coupling between electron temperature and electrostatic potential due to sheath currents leading to spin of filament structures. The calculations showed that the existing two-field model can be extended to the tree-field model. We have also showed that that the temperature field extends an energy theorem, but the mechanism of the interchange motions remains the same. This thesis may be considered as a first step to the three-field description of the filament motions in plasma.

Velocity scaling laws were also derived. It was shown, that the maximal center-of-mass velocity scales as a square root of the density amplitude only if this amplitude is small in comparison with the background density, for the amplitudes are large, the velocity scales as unity. It was also shown that in case of the constant background density the maximum centre-of-mass velocity scales as a square root of the temperature amplitude independently on the background temperature. These scaling laws were verified numerically by the two-dimensional advection-diffusion solver.

Contents

List of Figures

1

Introduction

Modern society has confronted with the constantly increasing energy demand, which is a vital and issue. Most of world's energy is currently produced from fossil fuels whichnare not renewable. This problem throws a challenge, force us in the future to switch to alternative energy sources. The number of conceivable non-fossil candidates which in the long-term could substantially contribute to energy production is very limited: renewables, nuclear fission (breeders) and nuclear fusion. Fusion is the least developed of the three, but has particularly valuable environmental and safety advantages and disposes of virtually inexhaustible resources. The reserves of the deuterium on the Earth can supply society with electricity for 150 billion years (assuming 1995 world energy consumption) [1], also it can help mankind to survive the solar Red Giant catastrophe [2].

In nuclear physics, nuclear fusion is a reaction in which two or more atomic nuclei come close enough to form one or more different atomic nuclei and subatomic particles (neutrons or protons). The difference in mass between the reactants and products is manifested as the release of large amounts of energy.

The second half of the XX century had become a period of the intensive development of the nuclear physics. It showed that the nuclear reactions can become a huge source of the energy from the small amount of fuel. First nuclear power plant was launched only 9 years after from the first nuclear bomb explosion, and the first thermonuclear weapon was tested in 1952. Experts were predicting that the first nuclear fusion reactors would appear in 1960-s, but unfortunately,

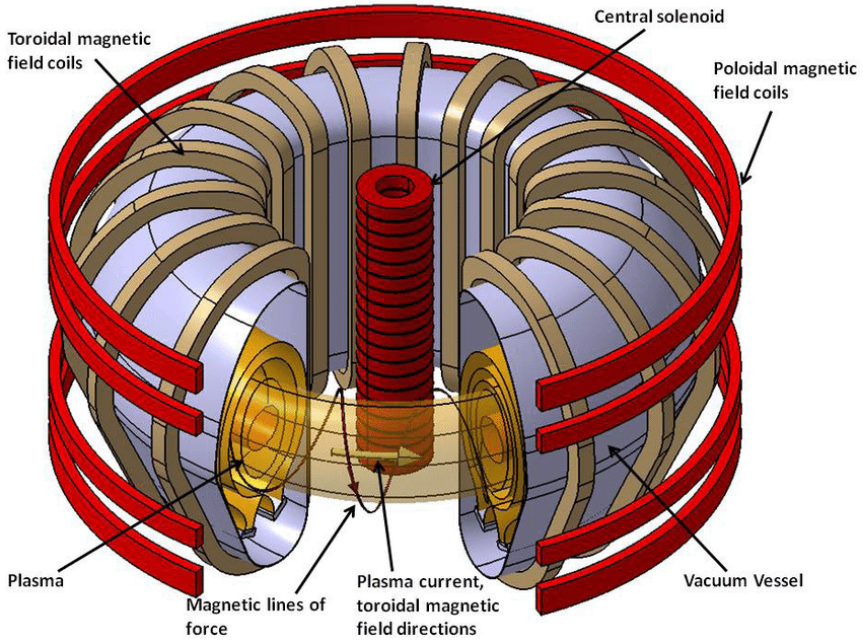

Figure 1.1: Principial scheme of tokamak [3].

these expectations were not delivered.

The biggest hope is now set on tokamak – its design suits best for the world's first fusion reactor. Tokamak is a device that generates a powerful magnetic field to confine high-temperature plasma in the shape of a torus. World's first tokamak, T-1, began operation in 1958 in the Soviet Union. In 1968, during the third IAEA International Conference on Plasma Physics and Controlled Nuclear Fusion Research at Novosibirsk, Soviet scientists announced that they had achieved electron temperatures of over 1000 eV in a tokamak device. These news were so miraculous, that at the beginning they were met with a big skepticism, since known fusion technologies were not able to approach that benchmark [4]. However, later it became clear that the designs of the powerful tokamaks that could provide a fusion energy, would be so expensive that they could not be developed by a single country. The initial agreement was made between Ronald Reagan and Mikhail Gorbachev in November 1985, and it became a starting point for ITER reactor – the primary international effort to develop practical fusion power.

Tokamak is a toroidal device which is designed to confine a high-temperature plasma using strong magnetic fields, see Figure 1.1. The principial magnetic field is toroidal and generated by the polloidal magnetic field coils. A toroidal electric current is induced in the plasma by a central solenoid. This current

induces a poloidal magnetic field which, together with the toroidal field, results in a helical magnetic field. This field contrains the charged particles in the plasma along helical paths within the vacuum chamber. This configuration of the magnetic fields does not completely avoid losses of plasma and heat across magnetic field lines. Plasma-wall interactions lead to erosion of the vessel walls and provide undesired impurities into the plasma. Such complicated configuration of the magnetic fields requires very detailed analysis of the different processes happening in the tokamak.

Usually three regions of the plasma interior in tokamaks are considered. The centre of the plasma is called plasma core, where the magnetic field lines lie on toroidal surfaces of constant pressure and are closed. This region is bordered by the scrape off layer (SOL). It is considered to be the small amount of residual plasma between the “edge” of the plasma and the tokamak vessel. In this region, the magnetic field lines intersect with the divertor plates. Transport in the SOL is very different from transport in the confined plasma due to the open field lines: it is predominantly convective [5].

In SOL particle densities and their temperatures are lower by several orders of magnitude than in the core plasma. Despite the divertor geometry some plasma will escape the magnetic confinement and may interact with the vessel wall. This transport across the magnetic field lines is dominated by the radial motion of filament structures. These structures contain excess particles and heat compared to the background plasma and are therefore referred as plasma blobs. The SOL absorbs most of the plasma exhaust (particles and heat) and transports it along the field lines to the divertor plates. Hence, this region is of prime importance for future reactors, and plasma dynamics in this region requires careful analysis. In this thesis we are going to analyze existing model equations for filament motions and extend them by including electron temperature dynamics.

This thesis consists of two parts: in the second chapter we present the derivation of the model equations that were used in the previous work and extend them by including electron temperature dynamics. We also present energy theorems and describe velocity scaling laws for both large and small relative amplitudes of the particle density and electron temperature oscillations. In the third chapter we describe the numerical methods that were used to solve model equations and test solver with the simple diffusion equation. We also provide the motivation for the optimal grid resolution and size of the simulation domain. Further we show how the dissipation coefficients affect the maximum center-of-mass velocity and then, after choosing the optimal parameters, verify numerically the velocity scaling laws that were derived in the previous part.

2

Model equations

In this chapter we derive reduced 2-field model equations that describe filament motions in case of isothermal electrons. We also derive an energy theorem for small density oscillation amplitudes and a velocity scaling law for this model. Then we extend our model to the three-field model assuming non-isothermal electrons. We also derive an energy theorem and velocity scaling laws for this three-field model.

2.1 Model setting

In this chapter we derive reduced 2-field model equations that describe filament motions in case of isothermal electrons. We also derive an energy theorem and a velocity scaling law for this model. Then we extend our model to the three-field model assuming non-isothermal electrons. We also derive an energy theorem and a velocity scaling laws for this three-field model.

2.2 Model setting

We consider a torus and introduce simple toroidal coordinates. The distance between the symmetry axis Z and the center of the circle that generates torus is R_0. Simple toroidal coordinates are (r, θ, ζ), where r is the minor radius, θ is

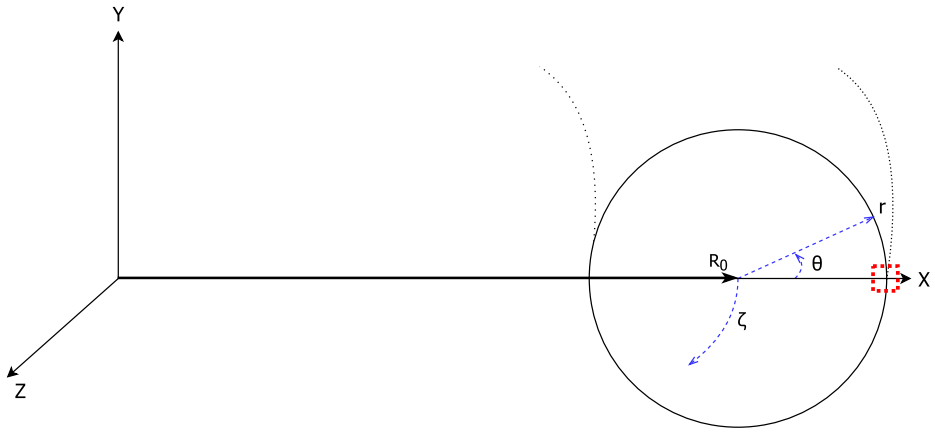

Figure 2.1: Simple torroidal coordinates.

called poloidal angle and gives an angle to the horizontal plane and ζ is called toroidal angle. These coordinates are defined by the transformation from the global Cartesian coordinates (X, Y, Z) as

$$r^2 = Y^2 + (X - R_0)^2, \quad \theta = \tan^{-1}\left(\frac{Y}{X - R_0}\right), \quad \zeta = \tan^{-1}\left(\frac{Z}{X}\right), \tag{2.1}$$

where $v = \sqrt{X^2 + Y^2} - R_0$ is the distance to the XZ-plane. The total distance from point to the symmetry axis is given by $R = R_0 + r\cos\theta$. The inverse transformation of the coordinates is then given by

$$X = (R_0 + r\cos\theta)\cos\zeta, \quad Y = r\sin\theta, \quad Z = (R_0 + r\cos\theta)\sin\zeta. \tag{2.2}$$

Unit vectors can be written as

$$\mathbf{e}_r = \cos(\theta)\cos(\zeta)\mathbf{e}_X + \sin(\theta)\mathbf{e}_Y + \cos(\theta)\sin(\zeta)\mathbf{e}_Z, \tag{2.3a}$$
$$\mathbf{e}_\theta = -\sin(\theta)\cos(\zeta)\mathbf{e}_X + \cos(\theta)\mathbf{e}_Y - \sin(\theta)\sin(\zeta)\mathbf{e}_Z, \tag{2.3b}$$
$$\mathbf{e}_\zeta = \sin(\zeta)\mathbf{e}_X + \cos(\zeta)\mathbf{e}_Z. \tag{2.3c}$$

This yields also that

$$\mathbf{e}_r \times \mathbf{e}_\theta = \mathbf{e}_\zeta, \quad \mathbf{e}_\theta \times \mathbf{e}_\zeta = \mathbf{e}_r, \quad \mathbf{e}_\zeta \times \mathbf{e}_r = \mathbf{e}_\zeta. \tag{2.4}$$

The gradient operator is given by

$$\nabla f = \frac{\partial f}{\partial r}\mathbf{e}_r + \frac{1}{r}\frac{\partial f}{\partial \theta}\mathbf{e}_\theta + \frac{1}{R}\frac{\partial f}{\partial \zeta}\mathbf{e}_\zeta, \tag{2.5}$$

and the curl is given by

$$\begin{aligned}\nabla \times \mathbf{F} = &\frac{1}{rR}\left(\frac{\partial}{\partial\theta}(rF_\zeta) - \frac{\partial}{\partial\zeta}(rF_\theta)\right)\mathbf{e}_r + \frac{1}{R}\left(\frac{\partial}{\partial\zeta}F_r - \frac{\partial}{\partial r}(RF_\zeta)\right)\mathbf{e}_\theta \\ &+ \frac{1}{r}\left(\frac{\partial}{\partial r}(rF_\theta - \frac{\partial}{\partial\theta}F_r)\right)\mathbf{e}_\zeta\end{aligned} \tag{2.6}$$

Simple torroidal coordinates approximate the magnetic geometry of torroidally confined plasmas by omitting the complicated description in terms of magnetic flux coordinates. The toroidal component of the magnetic field is not homogeneous and decreases as $1/R$ in the X-direction. Its inhomogenity induces ∇B that points in the opposite direction. The simulation domain of the filament structures is located at the edge of the torus in the radial-poloidal plane and is marked by dashed rectangle on Figure 2.1. The characteristic filament length will be of order 1 cm, while typical radius has length of meters [6].

2.2.1 Model setting

We will follow Kube [7], [8] closely to derive two-field reduced model equations for filament motions. We start from the fluid equations which describe the plasma [9], [10]. Further we denote particle species with index α, where $\alpha = e$ stands for electrons and $\alpha = i$ stands for ions. The continuity equation for particle species α, where inelastic collisions are neglected, is given by

$$\frac{\partial n_\alpha}{\partial t} + \nabla \cdot (n_\alpha \mathbf{u}_\alpha) = 0. \tag{2.7}$$

Here m_α denotes the mass of each of particle species α, n_α denotes its density and $\mathbf{u}_\alpha$ denotes the fluid parcels velocity.

The momentum equation is given by

$$m_\alpha n_\alpha \left(\frac{\partial}{\partial t} + \mathbf{u}_\alpha \cdot \nabla \right) \mathbf{u}_\alpha = -\nabla p_\alpha + q_\alpha n_\alpha (\mathbf{E} + \mathbf{u}_\alpha \times \mathbf{B}) - \nabla \cdot \boldsymbol{\pi}_\alpha - \sum_\beta m_\alpha n_\alpha \nu_{\alpha\beta} (\mathbf{u}_\alpha - \mathbf{u}_\beta), \tag{2.8}$$

where inelastic collisions are also neglected. Here q_α gives the particle charge, ($q_i = e$ and $q_e = -e$ are elementary charges for a simple plasma), p_α is the pressure and $\nu_{\alpha\beta}$ is the collision frequency between particle species α and β.

The set of all possible positions $\mathbf{x}$ and velocities $\mathbf{v}$ of the particle species is called the phase space of the system [11]. It is a set of three coordinates for each position coordinate (x, y, z) and three more for each velocity component (v_x, v_y, v_z). The entire space is 6-dimensional: a point in this space is $(x, v) = (x, y, z, v_z, v_y, v_z)$, and each coordinate is parameterized by time t. $f_\alpha(\mathbf{x}, \mathbf{v}, t)$ is a 6-dimensional probability density function defined so that

$$\mathrm{d}N = f_\alpha(\mathbf{x}, \mathbf{v}, t)\ \mathrm{d}^3\mathbf{x}\mathrm{d}^3\mathbf{v} \tag{2.9}$$

is the number of particle species α which all have positions lying within a small volume element $\mathrm{d}^3\mathbf{x}$ and having velocities in the range $\mathrm{d}^3\mathbf{v}$ at an instant time

moment t. We can integrate over a region of position space and momentum space to obtain the result that gives the total number of particles which have positions and momenta in that region. The velocity $\mathbf{v}$ can be represented as a sum of the directed velocity $\mathbf{u}$ and a random velocity $\mathbf{w}$:

$$\mathbf{v} = \mathbf{u} + \mathbf{w} \tag{2.10}$$

The viscous stress tensor for any given particle species is defined as

$$\pi_{ij} = mn\left\langle w_i w_j - \frac{w^2\delta_{ij}}{3}\right\rangle, \quad i,j \in \{1,2,3\}, \tag{2.11}$$

where δ_{ij} is the Kronecker tensor, defined by $\delta_{ij} = 1$ for $i = j$ and $\delta_{ij} = 0$ for $i \neq j$. $\langle \ldots \rangle$ denotes an average, defined by

$$\langle \mathbf{w} \rangle = \int \mathrm{d}\mathbf{v}\, \mathbf{w} f(\mathbf{x}, \mathbf{v}, t). \tag{2.12}$$

The energy equation is given by

$$\left(\frac{\partial}{\partial t} + \mathbf{u}_\alpha \cdot \nabla\right) p_\alpha + \frac{5}{3} p_\alpha \nabla \cdot \mathbf{u}_\alpha + \frac{2}{3}\boldsymbol{\pi} \cdot \nabla \cdot \mathbf{u}_\alpha + \frac{2}{3}\nabla \cdot \mathbf{q}_\alpha = 0, \tag{2.13}$$

where

$$\mathbf{q}_\alpha = \int \mathrm{d}\mathbf{w} \frac{1}{2} m_\alpha \mathbf{w}^2 \mathbf{w} f(\mathbf{x}, \mathbf{v}, t) \tag{2.14}$$

is the heat flux vector and inelastic collisions have been neglected.

We are going to make the following assumptions to simplify these equations and derive reduced two-field model equations.

1. We assume that the plasma contains only electrons and only one ion species, the latter for simplicity of notation is taken to be signly charged.

2. The state of plasma is a local thermodynamic equilibrium. It means that this state is defined by a phase space particle distribution function that everywhere has a normal distribution of its velocities, that is, a local Maxwellian distribution

$$f_\alpha(\mathbf{x}, \mathbf{v}, t) = \frac{n_\alpha(\mathbf{x}, t)}{(2\pi)^{\frac{3}{2}} \left[v_{th,\alpha}(\mathbf{x}, t)\right]^2} \exp\left(-\frac{[\mathbf{v} - \mathbf{u}_\alpha(\mathbf{x}, t)]^2}{2\left[v_{th,\alpha}(\mathbf{x}, t)\right]^2}\right), \tag{2.15}$$

where $\mathbf{v}_{th,\alpha}$ denotes the thermal velocity

$$v_{th,\alpha} = \left(\frac{T_\alpha}{m_\alpha}\right)^{1/2}, \tag{2.16}$$

and T_α denotes the temperature. Since this function is even in the random velocity, i.e.

$$f_\alpha(\mathbf{x}, \mathbf{u} + \mathbf{w}, t) = f_\alpha(\mathbf{x}, \mathbf{u} - \mathbf{w}, t), \tag{2.17}$$

it follows that the viscosity π_α defined by (2.11) vansishes.

3. The plasma is quasineutral, i.e. the plasma can be treated as being electrically neutral and space charges are not important [12]. Mathematically it means that charge density is

$$\varrho \equiv \sum_s n_s q_s = e(n_i - n_e) \approx 0 \tag{2.18}$$

and

$$\frac{\partial \varrho}{\partial t} \approx 0. \tag{2.19}$$

This also yields that electron and ion densities are equal to each other, i.e. $n_i \approx n_e \equiv n$.

4. Cold ions are assumed, i.e. $T_i \approx 0$. We also assume that the ion pressure gradient is given by $\nabla p_i = \nabla(nT_i) = 0$.

5. Electron inertia is neglected. The proton mass is given by $m_i = 1.6 \cdot 10^{-27}$ kg, the electron mass is given by $m_e = 9.1 \cdot 10^{-31}$ kg, and their ratio is $\frac{m_e}{m_i} = 1758$. We will therefore neglect the left hand side term of equation (2.8) for electrons.

6. Particle collisions are neglected, i.e. $\nu_{\alpha\beta} = 0$. This yields that the last term on the right hand side of equation (2.8) vanishes both for ions and electrons.

7. We neglect magnetic field due to the volume currents in the plasma [13], which according to Ampère's law implies

$$\mu_0 \mathbf{J} = \nabla \times \mathbf{B} = \nabla \times (B\mathbf{b}) = \nabla \times \mathbf{b} + \mathbf{b} \times \nabla \ln B = 0, \tag{2.20}$$

where

$$\mathbf{J} = \sum_\alpha q_\alpha n_\alpha \mathbf{u}_\alpha \tag{2.21}$$

denotes electric current density, μ_0 denotes magnetic permeability of vacuum, $\mathbf{B}$ denotes the magnetic field, B denotes the magnetic field strength and $\mathbf{B} = B\mathbf{b}$.

8. We are assuming a time-independent magnetic field both with respect to laboratory observer and along the fluid streamline, i.e.

$$\frac{\partial \mathbf{B}}{\partial t} = \mathbf{0}, \quad \frac{\mathrm{d}\mathbf{B}}{\mathrm{d}t} = \mathbf{0}. \tag{2.22}$$

9. Low-beta plasma is assumed. In plasma physics β is defined as the ratio of the pressure of the plasma to the magnetic energy density [14]

$$\beta = \frac{p}{p_m} = \frac{nT}{B^2/(2\mu_0)} \ll 1, \tag{2.23}$$

where p_m is the magnetic pressure.

10. We assume that parallel currents are incompressible, and therefore neglect the sheath dissipation.

$$\nabla_{\parallel} \cdot \mathbf{J}_{\parallel} = 0. \tag{2.24}$$

With these assumptions the momentum equation (2.8) can be written as

$$m_i n \left(\frac{\partial}{\partial t} + \mathbf{u}_i \cdot \nabla \right) \mathbf{u}_i = en(\mathbf{E} + \mathbf{u}_i \times \mathbf{B}), \tag{2.25a}$$

$$0 = -\nabla p_e - en(\mathbf{E} + \mathbf{u}_e \times \mathbf{B}) \tag{2.25b}$$

for the ions and electrons respectively. We multiply equations (2.25a) and (2.25b) with $\mathbf{b}\times$ and solve them for the perpendicular component of the velocity

$$\mathbf{u}_{i,\perp} = \frac{\mathbf{b} \times \nabla \phi}{B} + \frac{1}{\omega_{ci}} \mathbf{b} \times \frac{\mathrm{d}\mathbf{u}_i}{\mathrm{d}t}, \tag{2.26a}$$

$$\mathbf{u}_{e,\perp} = \frac{\mathbf{b} \times \nabla \phi}{B} - \frac{1}{neB} \mathbf{b} \times \nabla p_e, \tag{2.26b}$$

where $\omega_{ci} = eB/m_i$ denotes the ion cyclotron frequency. The contributions to the electron velocity (2.26b) are identified as the $\mathbf{E}\times\mathbf{B}$-drift and the diamagnetic drift respectively. The components of (2.26a) are identified as the $\mathbf{E} \times \mathbf{B}$-drift and the polarization drift respectively. The second term of the equation (2.26a) is of $O(\omega/\omega_{ci}^{-1})$. The typical magnitude of the magnetic field strength at SOL is 2 T, the typical frequency is 10^6 Hz [5], [15], so we evaluate $\omega_{ci} \approx 10^8$ Hz such that the contribution of the polarization drift gives higher order correction to the the contribution from the electric drift. Hence, we approximate the electron velocity $\mathbf{u}_i$ to the lowest order drift, and rewrite (2.26a) as

$$\mathbf{u}_{i,\perp} = \frac{\mathbf{b} \times \nabla \phi}{B} + \frac{1}{\omega_{ci}} \mathbf{b} \times \frac{\mathrm{d}\mathbf{u}_{\mathbf{E}\times\mathbf{B}}}{\mathrm{d}t}. \tag{2.27}$$

Using the definition of the electric charge density (2.18) and of the current densities (2.21) we write the particle continuity equation as

$$\frac{\partial \varrho}{\partial t} + \nabla \cdot \mathbf{J} = 0. \tag{2.28}$$

Assuming quasineutrality and incomprehensible parallel current we arrive at

$$\nabla \cdot \mathbf{J}_{\perp} = 0. \tag{2.29}$$

Substituting (2.26b) and (2.26a) into (2.29) we obtain

$$\nabla \cdot \mathbf{J}_\perp = \nabla \cdot (en\mathbf{u}_{pol,i} - en\mathbf{u}_{d,e}) = 0. \tag{2.30}$$

Observe that

$$\frac{\mathrm{d}\mathbf{u}_E}{\mathrm{d}t} = \frac{\mathrm{d}}{\mathrm{d}t}\left(\frac{\mathbf{E}\times\mathbf{B}}{B^2}\right) = \frac{\mathrm{d}\mathbf{E}}{\mathrm{d}t}\times\frac{\mathbf{b}}{B} + \cancelto{0}{\frac{\mathrm{d}\mathbf{b}}{\mathrm{d}t}}\times\frac{\mathbf{E}}{B} = \frac{\mathbf{b}}{B}\times\frac{\mathrm{d}\nabla_\perp\phi}{\mathrm{d}t}. \tag{2.31}$$

The first term of (2.30) can be written as

$$\begin{aligned}\nabla\cdot(ne\mathbf{u}_{i,pol}) &= \nabla\cdot\left(\frac{m_i n}{B}\mathbf{b}\times\frac{\mathrm{d}\mathbf{u}_E}{\mathrm{d}t}\right)\\ &= m_i\left(\frac{\nabla n}{B} - \frac{n\nabla\ln B}{B} + \frac{n}{B}\nabla\right)\cdot\left(\mathbf{b}\times\left[\frac{\mathbf{b}}{B}\times\frac{\mathrm{d}\nabla\phi}{\mathrm{d}t}\right]\right)\\ &= -\frac{m_i}{B^2}\left(\nabla n\cdot\frac{\mathrm{d}\nabla_\perp\phi}{\mathrm{d}t} - 2n\nabla\ln B\cdot\frac{\mathrm{d}\nabla_\perp\phi}{\mathrm{d}t} + n\frac{\mathrm{d}\nabla_\perp^2\phi}{\mathrm{d}t}\right).\end{aligned} \tag{2.32}$$

We estimate the length scale of the density perturbations to be $\nabla_\perp \ln n \sim \nabla_\perp \sim 1/l$. The magnetic field varies on a length scale given by the major radius, $\nabla_\perp \ln B \sim 1/R_0$. Since $R_0 \gg l$, the second term in (2.32) can be neglected. We will also use the Boussinesq approximation under which the spatial variations in the plasma density are assumed to be small compared to the variations of the electric potential [16]

$$\nabla n\cdot\frac{\mathrm{d}\nabla_\perp\phi}{\mathrm{d}t} \ll n\frac{\mathrm{d}\nabla_\perp^2\phi}{\mathrm{d}t}. \tag{2.33}$$

Hence, the compression of the ion polarization drift is approximated by

$$\nabla\cdot(en\mathbf{u}_{i,pol}) = -\frac{nm_i}{B^2}\frac{\mathrm{d}\nabla_\perp^2\phi}{\mathrm{d}t}. \tag{2.34}$$

The compression of the electric drift is given by

$$\begin{aligned}\nabla\cdot\mathbf{u}_{\mathbf{E}\times\mathbf{B}} &= \nabla\cdot\left(\frac{\mathbf{E}\times\mathbf{B}}{B^2}\right) = \nabla\cdot\left(\frac{1}{B}(\mathbf{E}\times\mathbf{b})\right)\\ &= \frac{1}{B}\nabla\cdot(\mathbf{E}\times\mathbf{b}) + (\mathbf{E}\times\mathbf{b})\cdot\nabla\left(\frac{1}{B}\right)\\ &= \frac{1}{B}(\nabla\times\mathbf{b} + \mathbf{b}\times\nabla\ln B)\cdot\nabla\phi\end{aligned} \tag{2.35}$$

Compression of the electron diamagnetic drift is:

$$\begin{aligned}\nabla\cdot(n\mathbf{u}_{d,i}) &= \nabla\cdot\left(n\left(-\frac{1}{eBn}\right)\mathbf{b}\times\nabla p_e\right) = \left(-\frac{1}{e}\right)\nabla\cdot\left(\frac{1}{B}\mathbf{b}\times\nabla p_e\right) =\\ &= -\frac{1}{eB}(\nabla\times\mathbf{b} + \mathbf{b}\times\nabla\ln B)\cdot\nabla p_e\end{aligned} \tag{2.36}$$

Now we can introduce a curvature operator

$$K(u) = \frac{1}{B}(\mathbf{b} \times \nabla \ln B + \nabla \times \mathbf{b}) \cdot \nabla u \tag{2.37}$$

Using different approximations and assumptions about the magnetic field we can obtain different contributions from this term. We consider a purely toroidal magnetic field in simple toroidal coordinate system, which is given as

$$\mathbf{B} = \frac{B_0 R_0}{R_0 + r\cos(\theta)} \mathbf{e}_\zeta. \tag{2.38}$$

This yields that $\mathbf{b} = \mathbf{e}_\zeta$. Using (2.5) and (2.6) we find that

$$\nabla \ln B = \frac{\nabla B}{B} = \frac{\cos\theta}{R}\mathbf{e}_r - \frac{\sin\theta}{R}\mathbf{e}_\theta, \tag{2.39}$$

$$\nabla \times \mathbf{b} = -\frac{1}{R}\sin\theta \mathbf{e}_r - \frac{1}{R}\cos\theta \mathbf{e}_\theta. \tag{2.40}$$

At the outboard midplane $\theta \approx 0$, so $\sin\theta \approx 0$, $\cos\theta \approx 1$, so the unit vector $\mathbf{e}_r$ according to (2.3b) is given by

$$\mathbf{e}_\theta \approx \mathbf{e}_y. \tag{2.41}$$

We can therefore multiply (2.39) with $\mathbf{b}\times$ and reduce (2.39) and (2.40) to

$$\mathbf{b} \times \nabla \ln B \approx \mathbf{e}_\zeta \times \frac{1}{R}\mathbf{e}_r = -\frac{1}{R}\mathbf{e}_\theta \rightarrow -\frac{1}{R}\mathbf{e}_y, \tag{2.42}$$

$$\nabla \times \mathbf{b} \approx -\frac{1}{R}\mathbf{e}_r \rightarrow -\frac{1}{R}\mathbf{e}_y \tag{2.43}$$

Here we have introduced local Cartesian coordinates, where

$$x = R - R_*, \qquad y = R_*\theta, \qquad z = R_*\zeta \tag{2.44}$$

and R_* simply denotes a point at R-axis which lies very closely to the SOL. Thus, we can rewrite the curvature operator as

$$K(u) = -\frac{1}{B}\left(\frac{2}{R}\mathbf{e}_y\right) \cdot \nabla u = -\frac{2}{BR}\frac{\partial u}{\partial y}. \tag{2.45}$$

We will also approximate B and R as

$$B \approx B_0, \quad R \approx R_0. \tag{2.46}$$

The compressions of the electron $\mathbf{E}\times\mathbf{B}$-drift and diamagnetic drift are therefore given by

$$\nabla \cdot \mathbf{u}_{\mathbf{E}\times\mathbf{B}} = -\frac{2}{B_0 R_0}\frac{\partial \phi}{\partial y}, \tag{2.47}$$

$$\nabla \cdot (-ne\mathbf{u}_{d,e}) = \frac{2T_e}{B_0 R_0}\frac{\partial n}{\partial y}. \tag{2.48}$$

Our next step will be an introduction of plasma vorticity. Observe that curl of $u_{\mathbf{E}\times\mathbf{B}}$ is

$$\begin{aligned}\nabla \times \mathbf{u}_{\mathbf{E}\times\mathbf{B}} &= \nabla \times \left(\frac{1}{B}\mathbf{b} \times \nabla\phi\right) \\ &= \frac{1}{B}(\nabla \cdot \nabla\phi)\mathbf{b} - \nabla\phi\left(\nabla \cdot \frac{1}{B}\mathbf{b}\right) + (\nabla\phi \cdot \nabla)\frac{1}{B}\mathbf{b} - \left(\frac{1}{B}\mathbf{b} \cdot \nabla\right)\phi \quad (2.49)\end{aligned}$$

On the similar way as we did in (2.32) we will use the fact that the characteristic length scale of the magnetic field is R_0 and of the electric potential is l, and $l << R_0$. It will let us drop second, third and fourth term of (2.49). Therefore we approximate the vorticity as

$$\Omega \equiv \mathbf{b} \cdot \nabla \times \mathbf{u}_{\mathbf{E}\times\mathbf{B}} = \mathbf{b} \cdot \nabla \times \left(\frac{1}{B}\mathbf{b} \times \nabla\phi\right) \approx \frac{1}{B_0}\nabla_\perp^2\phi. \quad (2.50)$$

Now we can rewrite (2.30) as

$$\frac{B_0}{nm_i}\nabla \cdot \mathbf{J}_\perp = \frac{\mathrm{d}\Omega}{\mathrm{d}t} + \frac{2T_e}{R_0 n m_i}\frac{\partial n}{\partial y} = 0. \quad (2.51)$$

Observe that the advective derive is given as

$$\frac{\mathrm{d}}{\mathrm{d}t} = \left(\frac{\partial}{\partial t} + \mathbf{u}_E \cdot \nabla\right) = \left(\frac{\partial}{\partial t} + \frac{\mathbf{b} \times \nabla\phi}{B} \cdot \nabla\right). \quad (2.52)$$

We introduce Poisson brackets

$$\{\phi, f\} = \frac{\partial\phi}{\partial x}\frac{\partial f}{\partial y} - \frac{\partial\phi}{\partial y}\frac{\partial f}{\partial x} \quad (2.53)$$

and define ion acoustic velocity as $C_s = \sqrt{T_e/m_i}$. Then we rewrite vorticity equation (2.51) as

$$\frac{\partial\Omega}{\partial t} + \frac{1}{B_0}\{\phi, \Omega\} + \frac{2C_s^2}{R_0 n}\frac{\partial n}{\partial y} = 0. \quad (2.54)$$

In order to obtain a set of normalized equations we perform a normalization. Let

$$t \to \hat{t} = \gamma t, \quad \mathbf{x} \to \hat{\mathbf{x}} = \frac{\mathbf{x}}{l}, \quad \nabla \to \hat{\nabla} = \nabla l, \quad \phi \to \hat{\phi} = \frac{\phi}{\gamma B_0 l^2}, \quad n \to \hat{n} = \frac{n}{\mathcal{N}}, \quad (2.55)$$

where γ is a characteristic frequency, l is a characteristic length and $\mathcal{N}$ is a characteristic particle density. Then (2.54) can be rewritten as

$$\left(\gamma\frac{\partial}{\partial\hat{t}} + \frac{1}{B_0}\hat{\mathbf{b}} \times \frac{\hat{\nabla}}{l}\hat{\phi}\gamma B l^2 \cdot \frac{\hat{\nabla}}{l}\right)\frac{\hat{\nabla}^2}{l^2}\gamma B_0 l^2\hat{\phi} + \frac{2C_s^2}{R_0 l}\frac{\partial\hat{n}}{\partial\hat{y}} = 0, \quad (2.56)$$

which gives

$$\frac{\partial \hat{\nabla}_\perp^2 \phi}{\partial \hat{t}} + \{\hat{\phi}, \hat{\nabla}_\perp^2 \hat{\phi}\} + \frac{2C_s^2}{\gamma^2 R_0 l} \frac{1}{\hat{n}} \frac{\partial \hat{n}}{\partial \hat{y}} = 0. \tag{2.57}$$

We can choose the characteristic frequency to be

$$\gamma = \sqrt{2\frac{C_s^2}{R_0 l}}, \tag{2.58}$$

which is identified as an ideal interchange rate, and define normalized vorticity as

$$\hat{\Omega} = \hat{\nabla}^2 \hat{\phi} \tag{2.59}$$

to end up with the normalized dimensionless vorticity equation

$$\frac{\partial \hat{\Omega}}{\partial \hat{t}} + \{\hat{\phi}, \hat{\Omega}\} + \frac{\partial \ln \hat{n}}{\partial \hat{y}} = 0. \tag{2.60}$$

We substitute the perpendicular component of the electron velocity (2.26b) into the electron continuity equation (2.7) and, using curvature operator (2.45), obtain

$$\frac{\partial n}{\partial t} + \nabla \cdot (n \mathbf{u}_{\mathbf{E}\times\mathbf{B}}) + \nabla \cdot (n \mathbf{u}_{d,i}) = 0, \tag{2.61}$$

$$\left(\frac{\partial}{\partial t} + \frac{\mathbf{b}}{B_0} \times \nabla\phi \cdot \nabla\right) n - \frac{2n}{B_0 R_0} \frac{\partial \phi}{\partial y} - \frac{2T_e}{eB_0 R_0} \frac{\partial n}{\partial y} = 0. \tag{2.62}$$

The normalized continuity equation is

$$\gamma \left(\frac{\partial}{\partial \hat{t}} + \frac{1}{B_0}\mathbf{b} \times \frac{\hat{\nabla}}{l}\hat{\phi}\gamma B l^2 \cdot \frac{\hat{\nabla}}{l}\right) \mathcal{N}\hat{n} - \frac{2\mathcal{N}\hat{n}}{B_0 R_0} \frac{\gamma B l^2}{l} \frac{\partial \hat{\phi}}{\partial \hat{y}} - \frac{2T_e}{B_0 R_0 e} \frac{\mathcal{N}}{l} \frac{\partial \hat{n}}{\partial \hat{y}} = 0, \tag{2.63}$$

$$\frac{\partial \hat{n}}{\partial \hat{t}} + \{\hat{\phi}, \hat{n}\} - \frac{2l}{R_0}\hat{n}\frac{\partial \hat{\phi}}{\partial \hat{y}} - \frac{2T_e}{e\gamma B_0 R_0} \frac{1}{l} \frac{\partial \hat{n}}{\partial \hat{y}} = 0, \tag{2.64}$$

$$\frac{\partial \ln \hat{n}}{\partial \hat{t}} + \{\hat{\phi}, \ln \hat{n}\} - \frac{2l}{R_0} \frac{\partial \hat{\phi}}{\partial \hat{y}} - \frac{2C_s^2}{\gamma \omega_{ci} R_0 l} \frac{\partial \ln \hat{n}}{\partial \hat{y}} = 0 \tag{2.65}$$

We neglect the compression of the electric drift since $l \ll R_0$. The typical SOL- and blob parameters are according to [15]

$$R \approx 2 \text{ m}, \quad T_e \sim 50 \text{ eV} \approx 6 \cdot 10^5 \text{ K}, \quad l \approx 10^{-2}\text{m}, \quad B_0 \sim 2 \text{ T}$$

We can therefore estimate the coefficient of the last term of (2.65), which is $\frac{2C_s^2}{\gamma \omega_{ci} R_0 l} \approx 10^{-3}$. Therefore, the coefficient of the compression of the diamagnetic flux can be neglected. Previous numerical studies have also shown that

this term has a small contribution into the cross-field dynamic [17]. Therefore, the two-field model equations are

$$\frac{\partial \ln \hat{n}}{\partial \hat{t}} + \{\phi, \ln \hat{n}\} = 0, \tag{2.66}$$

$$\frac{\partial \hat{\Omega}}{\partial \hat{t}} + \{\hat{\phi}, \hat{\Omega}\} + \frac{\partial \ln \hat{n}}{\partial \hat{y}} = 0, \tag{2.67}$$

$$\hat{\Omega} = \hat{\nabla}_{\perp}^2 \hat{\phi} \tag{2.68}$$

Equation (2.66) describes the advection of the density with the electric drift, equation (2.67) is a vorticity equation that was derived from the compression of the electric current. The closure of these equation is provided by vorticity. There are no free model parameters, so the length scale of the blob is the only length scale in this model. It will allow us to derive the velocity scaling law without solving the model equations.

Further in this study we assume that the density is given as a sum of the constant background density and fluctuation

$$n(x, y, t) = \mathcal{N} + \Delta n \, n'(x, y, t) \tag{2.69}$$

where n' denotes perturbed part and Δn is a perturbation amplitude. The normalized density is therefore given as

$$\hat{n} = 1 + \frac{\Delta n}{\mathcal{N}} \hat{n}' \tag{2.70}$$

For small density perturbations $\frac{\Delta n}{\mathcal{N}} \ll 1$ we can approximate last term of (2.67) as

$$\frac{1}{\hat{n}} \frac{\partial \hat{n}}{\partial \hat{y}} = \frac{\partial \hat{n}'}{\partial \hat{y}}, \tag{2.71}$$

so model equations can be written as

$$\frac{\partial \hat{n}'}{\partial \hat{t}} + \{\phi, \hat{n}'\} = 0, \tag{2.72}$$

$$\frac{\partial \hat{\Omega}}{\partial \hat{t}} + \{\hat{\phi}, \hat{\Omega}\} + \frac{\partial \hat{n}'}{\partial \hat{y}} = 0. \tag{2.73}$$

This model is known as a minimal model for interchange motions and is valid for density oscillations of the small order.

2.3 Energy theorem for isothermal ions

We will follow Kube et. al. [18]. In order to analyze the energy dynamics in the model described by equations (2.66)-(2.67) we consider a rectangle domain with lengths L_x and L_y in the local Cartesian coordinate system. We assume periodic boundary conditions for electric potential $\hat{\phi}$ and density $\hat{n}$, i.e.

$$\hat{u}(0,\hat{y}) = \hat{u}(L_x,\hat{y}), \quad \hat{u}(0,\hat{y}) = \hat{u}(L_x,\hat{y}) \qquad \text{for } \hat{u} = \hat{\phi} \text{ and } \hat{u} = \hat{n}. \tag{2.74}$$

We also assume that the functions $\hat{n}$ and $\hat{\phi}$ are smooth, so their derivatives are also periodic. For convenience we will use $\int \mathrm{d}\hat{A} = \frac{1}{L_x L_y} \int_0^{L_x}\int_0^{L_y} \mathrm{d}\hat{x}\mathrm{d}\hat{y}$ to denote integration over the domain. In local Cartesian coordinates the steam flow is associated with $\mathbf{E}\times\mathbf{B}$-drift, so

$$\hat{\mathbf{v}} = \mathbf{b}\times\hat{\nabla}\hat{\phi} = -\frac{\partial\hat{\phi}}{\partial\hat{y}}\mathbf{e}_x + \frac{\partial\hat{\phi}}{\partial\hat{x}}\mathbf{e}_y. \tag{2.75}$$

We can therefore define the kinetic energy as

$$\hat{E}_k = \int \mathrm{d}\hat{A}\, \hat{n}(\hat{\nabla}\hat{\phi})^2. \tag{2.76}$$

To obtain a kinetic energy equation we multiply (2.66) with $\frac{1}{2}\int \mathrm{d}\hat{A}\ (\hat{\nabla}_\perp\hat{\phi})^2$ and (2.67) with $\int \mathrm{d}\hat{A}\,\hat{n}\hat{\phi}$ respectively and get

$$\frac{1}{2}\int \mathrm{d}\hat{A}\ (\hat{\nabla}_\perp\hat{\phi})^2\frac{\partial\hat{n}}{\partial\hat{t}} + \frac{1}{2}\int \mathrm{d}\hat{A}\ (\hat{\nabla}_\perp\hat{\phi})^2\{\hat{\phi},\hat{n}\} = 0, \tag{2.77}$$

$$\int \mathrm{d}\hat{A}\,\hat{n}\hat{\phi}\frac{\partial(\hat{\nabla}^2_\perp\hat{\phi})}{\partial\hat{t}} + \int \mathrm{d}\hat{A}\,\hat{\phi}\hat{n}\{\hat{\phi},\hat{\nabla}^2_\perp\hat{\phi}\} + \int \mathrm{d}\hat{A}\,\hat{\phi}\frac{\partial\hat{n}}{\partial\hat{y}} = 0. \tag{2.78}$$

The first term of (2.78) can be written as

$$\int \mathrm{d}\hat{A}\,\hat{n}\hat{\phi}(\hat{\nabla}^2_\perp\hat{\phi}) = \cancelto{0}{\int \mathrm{d}\hat{A}\hat{\nabla}\cdot\left[\hat{n}\hat{\phi}\frac{\partial\hat{\nabla}_\perp\hat{\phi}}{\partial\hat{t}}\right]} - \int \mathrm{d}\hat{A}\ \hat{\nabla}(\hat{n}\hat{\phi})\frac{\partial\hat{\nabla}_\perp\hat{\phi}}{\partial\hat{t}} =$$

$$= -\int \mathrm{d}\hat{A}\ \hat{\phi}\hat{\nabla}\hat{n}\frac{\partial\hat{\nabla}_\perp\hat{\phi}}{\partial\hat{t}} - \frac{1}{2}\int \mathrm{d}\hat{A}\,\hat{n}\frac{\partial}{\partial\hat{t}}(\hat{\nabla}_\perp\hat{\phi})^2. \tag{2.79}$$

Using Leibniz's rule we find that the second term of (2.78) can be written as

$$\int \mathrm{d}\hat{A}\,\hat{\phi}\hat{n}\{\hat{\phi},\hat{\nabla}^2_\perp\hat{\phi}\} = \frac{1}{2}\int \mathrm{d}\hat{A}\,\hat{n}\{\hat{\phi}^2,\hat{\nabla}^2_\perp\hat{\phi}\}. \tag{2.80}$$

We subtract equation (2.78) from (2.77) and obtain

$$\frac{\mathrm{d}\hat{E}_k}{\mathrm{d}\hat{t}} + \int \mathrm{d}\hat{A}\,\hat{\phi}\hat{\nabla}\hat{n}\frac{\partial\hat{\nabla}_\perp\hat{\phi}}{\partial\hat{t}}$$

$$-\frac{1}{2}\int \mathrm{d}\hat{A}\ \left(\hat{n}\{\hat{\phi}^2,\hat{\nabla}^2_\perp\hat{\phi}\} - (\hat{\nabla}_\perp\hat{\phi})^2\{\hat{\phi},\hat{n}\}\right) + \int \mathrm{d}\hat{A}\,\hat{n}\frac{\partial\hat{\phi}}{\partial\hat{y}} = 0. \tag{2.81}$$

This result yields that we cannot derive the energy theorem for model equations (2.66)-(2.67). The reason is that we cannot cancel the second term of (2.81). To do that we have to call off the Boussinesq approximation and include the spatial variations in the plasma density to the polarization drift and extend the polarization drift (2.32), but this extension would change the vorticity equation and involve complicated calculations that are not the part of the current project.

If we instead consider low-density oscillations described by the model equations (2.72)-(2.73), and that the density is given by (2.70), then the kinetic energy can be approximated to

$$\hat{E}_k = \int \mathrm{d}\hat{A}\, (\hat{\nabla}\hat{\phi})^2. \tag{2.82}$$

We can therefore multiply equation (2.73) with $\int \mathrm{d}\hat{A}\, \hat{\phi}$ and arrive at

$$\int \mathrm{d}\hat{A}\, \hat{\phi}\frac{\partial \hat{\nabla}_\perp^2 \hat{\phi}}{\partial \hat{t}} + \int \mathrm{d}\hat{A}\, \hat{\phi}\{\hat{\phi}, \hat{\nabla}_\perp^2 \hat{\phi}\} + \int \mathrm{d}\hat{A}\, \hat{\phi}\frac{\partial \hat{n}'}{\partial \hat{y}} = 0. \tag{2.83}$$

The first term of (2.83) is given as

$$\begin{aligned}\int \mathrm{d}\hat{A}\, \phi\frac{\partial \hat{\nabla}_\perp^2 \hat{\phi}}{\partial \hat{t}} &= \int \mathrm{d}\hat{A}\, \frac{\partial}{\partial \hat{t}}(\hat{\phi}\cdot \hat{\nabla}_\perp^2 \hat{\phi}) - \int \mathrm{d}\hat{A}\, \frac{\partial \hat{\phi}}{\partial \hat{t}}\hat{\nabla}_\perp^2 \hat{\phi} \\ &= \int \mathrm{d}\hat{A}\, \hat{\nabla}_\perp \cdot (\hat{\phi}\hat{\nabla}_\perp \hat{\phi}) - \int \mathrm{d}\hat{A}\, \hat{\phi}\frac{\partial \hat{\nabla}_\perp^2 \hat{\phi}}{\partial \hat{t}} - \int \mathrm{d}\hat{A}\, \hat{\nabla}_\perp^2 \hat{\phi}\frac{\partial \hat{\phi}}{\partial \hat{t}}\end{aligned} \tag{2.84}$$

The second term of (2.83) is

$$\int \mathrm{d}\hat{A}\, \hat{\phi}\{\hat{\phi}, \hat{\nabla}_\perp^2 \hat{\phi}\} = \int \mathrm{d}\hat{A}\, \left[\frac{\partial}{\partial \hat{y}}\left(\hat{\phi}^2 \frac{\partial \hat{\nabla}_\perp^2 \hat{\phi}}{\partial \hat{x}}\right) - \frac{\partial}{\partial \hat{x}}\left(\hat{\phi}^2 \frac{\partial \hat{\nabla}_\perp^2 \hat{\phi}}{\partial \hat{y}}\right)\right] = 0. \tag{2.85}$$

The third term of (2.83)

$$\int \mathrm{d}\hat{A}\, \hat{\phi}\frac{\partial \hat{n}'}{\partial \hat{y}} = -\int \mathrm{d}\hat{A}\, \hat{n}\frac{\partial \hat{\phi}}{\partial \hat{y}} = -\int \mathrm{d}\hat{A}\, \hat{n}\hat{v}_{\hat{x}} \equiv -\Gamma_{\hat{n}} \tag{2.86}$$

is associated with the particle flux $\Gamma_{\hat{n}}$ transports particle through the surface. We can therefore write (2.83) as

$$\frac{\mathrm{d}\hat{E}_k}{\mathrm{d}t} = \int \mathrm{d}\hat{A}\, \hat{n}\frac{\partial \hat{\phi}}{\partial \hat{y}} \equiv \Gamma_{\hat{n}} \tag{2.87}$$

We define potential energy of the plasma in its effective gravity field as

$$\hat{E}_p = \int \mathrm{d}\hat{A}\, \hat{x}\hat{n}. \tag{2.88}$$

To obtain an energy equation we multiply (2.66) with $\hat{n}\int \mathrm{d}\hat{A}\, \hat{x}$ and obtain

$$\int \mathrm{d}\hat{A}\, \hat{x}\frac{\partial \hat{n}}{\partial \hat{t}} + \int \mathrm{d}\hat{A}\, \hat{x}\{\hat{\phi}, \hat{n}\} = 0. \tag{2.89}$$

We rewrite first term of (2.89) as

$$\int \mathrm{d}\hat{A}\,\hat{x}\frac{\partial \hat{n}}{\partial \hat{t}} = \frac{\partial}{\partial \hat{t}}\int \mathrm{d}\hat{A}\hat{x}\hat{n}' = \frac{\partial \hat{E}_p}{\partial \hat{t}}. \tag{2.90}$$

The second term of (2.89) is

$$\begin{aligned}\int \mathrm{d}\hat{A}\,\hat{x}\{\hat{\phi},\hat{n}\} &= \int \mathrm{d}\hat{A}\,\hat{x}\frac{\partial}{\partial \hat{y}}\left(\hat{\phi}\frac{\partial \hat{n}}{\partial \hat{x}}\right) - \int \mathrm{d}\hat{A}\,\hat{x}\frac{\partial}{\partial \hat{x}}\left(\hat{\phi}\frac{\partial \hat{n}}{\partial \hat{y}}\right)\\ &= -\int \mathrm{d}\hat{A}\,\hat{\phi}\frac{\partial \hat{n}}{\partial \hat{y}} = \int \mathrm{d}\hat{A}\,\hat{n}\frac{\partial \hat{\phi}}{\partial \hat{y}}.\end{aligned} \tag{2.91}$$

Equation (2.89) can therefore be written as

$$\frac{\mathrm{d}\hat{E}_p}{\mathrm{d}\hat{t}} = -\Gamma_{\hat{n}}. \tag{2.92}$$

We multiply (2.67) with $\int \mathrm{d}\hat{A}\,\hat{n}\hat{\phi}$ and obtain

$$\int \mathrm{d}\hat{A}\,\hat{n}\hat{\phi}\frac{\partial \hat{\nabla}_\perp^2 \hat{\phi}}{\partial \hat{t}} + \int \mathrm{d}\hat{A}\,\hat{n}\hat{\phi}\{\hat{\phi},\hat{\Omega}\} + \int \mathrm{d}\hat{A}\,\hat{\phi}\frac{\partial \hat{n}}{\partial \hat{y}} = 0. \tag{2.93}$$

We derive at the energy theorem by taking the sum of (2.83) and (2.89), which is

$$\frac{\mathrm{d}}{\mathrm{d}\hat{t}}(\hat{E}_k + \hat{E}_p) = 0. \tag{2.94}$$

This result yields that the sum of the potential and the kinetic energy is a conserved quantity. Energy theorem helps us to understand the interchange mechanism of the blob dynamics. Both curvature $\mathcal{K}$ and the magnetic field gradient $\hat{\nabla}\ln B$ cause guiding center drifts and lead to the polarization of the current. The polarized blob structure is then advected radially outwards, i.e. along the major radius R by the $\mathbf{E}\times\mathbf{B}$-drift, which is uniform regardless of particle charge. Assume that the initial conditions are given by

$$\hat{\phi}(\hat{t}=0) = 0, \tag{2.95a}$$

$$\hat{\Omega}(\hat{t}=0) = 0, \tag{2.95b}$$

$$\hat{n}(\hat{t}=0) = 1 + \frac{\Delta n}{\mathcal{N}}\exp\left(-\frac{\mathbf{x}^2}{2}\right). \tag{2.95c}$$

Then initially there is no kinetic energy in the blob, it has only potential energy in its effective gravity field. This potential energy transforms into the kinetic energy through the particle flux. We can summarize this conclusion and show the interchange mechanism on the Figure 2.2.

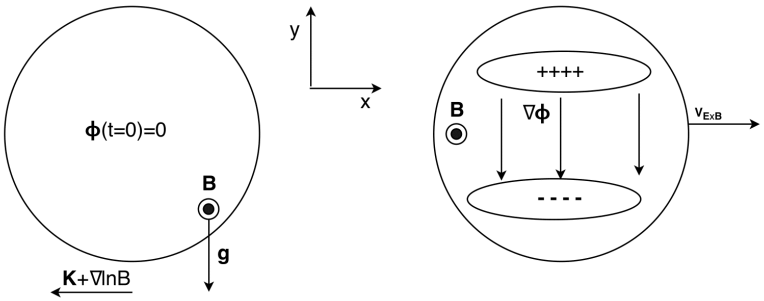

Figure 2.2: The illustration of the mechanism of the density blob in a magnetized plasma. The blob is initialized with the density oscillations (on the left) gets polarized, and starts moving radially outwards by $\mathbf{E} \times \mathbf{B}$-drift (on the right).

2.4 Velocity scaling law for isothermal electrons

Model vorticity equation is

$$\frac{\mathrm{d}\hat{\Omega}}{\mathrm{d}\hat{t}} + \frac{1}{\hat{n}}\frac{\partial \hat{n}}{\partial \hat{y}} = 0. \tag{2.96}$$

We will also assume that the density is given as a sum of the constant background density and oscillating part

$$\hat{n} = 1 + \frac{\Delta n}{\mathcal{N}}\hat{n}'. \tag{2.97}$$

Normalized vorticity is defined as

$$\hat{\Omega} = \mathbf{b} \cdot \hat{\nabla} \times \hat{\mathbf{u}}_{\mathbf{E}\times\mathbf{B}}, \tag{2.98}$$

so the first term of equation (2.96) scales as

$$\frac{\mathrm{d}\hat{\Omega}}{\mathrm{d}\hat{t}} \sim \hat{\gamma}\frac{\hat{V}}{\hat{l}} \sim \gamma\frac{\hat{V}}{\hat{l}}\frac{\hat{l}}{\hat{l}} \sim \frac{\hat{V}^2}{\hat{l}^2} \sim \hat{V}^2, \tag{2.99}$$

where we have used the fact that $\hat{l} = 1$. The second term of (2.96) scales as

$$\frac{1}{\hat{n}}\frac{\partial \hat{n}}{\partial \hat{y}} \sim \frac{1}{\hat{l}}\frac{\Delta n/\mathcal{N}}{1 + \Delta n/\mathcal{N}}. \tag{2.100}$$

Since $\hat{l} = 1$, we conclude that the normalized velocity scales as

$$\hat{V}^2 \sim \frac{\Delta n/\mathcal{N}}{1 + \Delta n/\mathcal{N}}. \tag{2.101}$$

In dimensional units velocity is given as

$$\hat{V}^2 = \frac{V^2}{l^2\gamma^2}. \tag{2.102}$$

Then, using characteristic frequency (2.58) we find that in dimensional units velocity scales as

$$V^2 \sim \gamma^2 l^2 \frac{\Delta n/\mathcal{N}}{1+\Delta n/\mathcal{N}} \sim \frac{2C_s^2}{R_0 l} l^2 \frac{\Delta n/\mathcal{N}}{1+\Delta n/\mathcal{N}} \sim C_s^2 \frac{2l}{R_0} \frac{\Delta n/\mathcal{N}}{1+\Delta n/\mathcal{N}}, \tag{2.103}$$

or

$$\frac{V}{C_s} \sim \left(\frac{2l}{R_0} \frac{\Delta n/\mathcal{N}}{1+\Delta n/\mathcal{N}}\right)^{1/2}, \tag{2.104}$$

It should be also noted that since model has no free parameters, this scaling is the only allowable scaling according to the dimensional analysis.

Is the oscillation amplitude is small, i.e. $\frac{\Delta n}{\mathcal{N}} \ll 1$, the velocity scaling (2.101) changes to

$$\hat{V} \sim \left(\frac{\Delta n}{\mathcal{N}}\right)^{1/2}. \tag{2.105}$$

If the oscillation amplitude is large, i.e. $\frac{\Delta n}{\mathcal{N}} \gg 1$, the velocity scaling (2.101) becomes

$$\hat{V} \sim 1, \tag{2.106}$$

i.e. velocity scales as unity independently of the amplitude.

2.5 Electron temperature dynamics

We extend the model by including the electron temperature dynamics, following Garcia et al [19]. It yields that electrons are no longer isothermal, and the electron pressure gradient is given by

$$\nabla p_e = n\nabla T_e + T_e \nabla n. \tag{2.107}$$

It yields that that the compression of the diamagnetic drift (2.36) is given by

$$\nabla \cdot (n\mathbf{u}_{d,e}) = -\frac{1}{e}\mathcal{K}(nT) = -\frac{1}{e}(T\mathcal{K}(n) + n\mathcal{K}(T)), \tag{2.108}$$

where e-index is dropped for convenience. Using (2.35) and (2.108) we write electron continuity equation (2.61) as

$$\left(\frac{\partial}{\partial t} + \frac{\mathbf{b}}{B_0} \times \nabla\phi \cdot \nabla\right) n + n\mathcal{K}(\phi) - \frac{1}{e}\left(n\mathcal{K}(T) + T\mathcal{K}(n)\right) = 0, \tag{2.109}$$

$$\frac{\partial n}{\partial t} + \frac{1}{B_0}\{\phi, n\} - \frac{2n}{B_0 R_0}\frac{\partial \phi}{\partial y} + \frac{2}{e}\frac{n}{B_0 R_0}\frac{\partial T}{\partial y} + \frac{2}{e}\frac{T}{B_0 R_0}\frac{\partial n}{\partial y} = 0. \tag{2.110}$$

The vorticity equation (2.30) becomes

$$n\left(\frac{\partial}{\partial t}+\frac{\mathbf{b}}{B_0}\times\nabla\phi\cdot\nabla\right)\Omega-\frac{B_0T}{m_i}\mathcal{K}(n)-\frac{nB_0}{m_i}\mathcal{K}(T)=0, \tag{2.111}$$

$$n\frac{\partial\Omega}{\partial t}+\frac{n}{B_0}\{\phi,\Omega\}+\frac{2T}{R_0m_i}\frac{\partial n}{\partial y}+\frac{2n}{m_iR_0}\frac{\partial T}{\partial y}=0. \tag{2.112}$$

We will also change our assumption about the Local Thermodynamic Equilibrium state. We assume instead that the viscous stress tensor equals zero $\boldsymbol{\pi}=0$ and use the 13th moment approximation for heat flux tensor. It can be shown [20] that this approximation provides a closure of the fluid equations by giving the following relation for the heat flow vector

$$\frac{5}{2}\frac{p}{m_i}\nabla T=\omega_{ce}\mathbf{q}\times\mathbf{b}. \tag{2.113}$$

We multiply (2.113) with $\mathbf{b}\times$ and obtain an equation for the perpendicular component of $\mathbf{q}$, which is

$$\mathbf{q}_\perp=-\frac{5}{2}\frac{nT}{eB}\times\nabla T. \tag{2.114}$$

Hence, the perpendicular component of the electron energy equation (2.13) is given by

$$\frac{3}{2}n\left(\frac{\partial}{\partial t}+\mathbf{u}_{e,\perp}\cdot\nabla\right)T+p\nabla\cdot\mathbf{u}_{e,\perp}+\nabla\cdot\mathbf{q}_\perp=0. \tag{2.115}$$

The second term of (2.115) is

$$\begin{aligned}\frac{3}{2}n\mathbf{u}_{e,\perp}\cdot\nabla T&=\frac{3}{2}n\left(\frac{\mathbf{b}}{B}\times\nabla\phi\right)\cdot\nabla T-\frac{3}{2e}\frac{1}{B}\mathbf{b}\times\nabla p_e\cdot\nabla T\\&=\frac{3}{2}\frac{n}{B}(\mathbf{b}\times\nabla\phi)\cdot\nabla T-\frac{3T}{2eB}\mathbf{b}\cdot\nabla n\times\nabla T.\end{aligned} \tag{2.116}$$

The third term of (2.115) is

$$\begin{aligned}nT\nabla\cdot\mathbf{u}_{e,\perp}&=nT\nabla\cdot\mathbf{u}_{\mathbf{E}\times\mathbf{B}}+nT\nabla\left(-\frac{1}{enB}\mathbf{b}\times\nabla p_e\right)\\&=-nT\mathcal{K}(\phi)+\frac{T}{e}\mathcal{K}(p)-\frac{T}{eB}\mathbf{b}\cdot\nabla n\times\nabla T.\end{aligned} \tag{2.117}$$

The compression of the perpendicular component of the heat flux vector is

$$\begin{aligned}\nabla\cdot\mathbf{q}_\perp&=-\frac{5}{2}\nabla\cdot\left[\left(\frac{nT}{B}\mathbf{b}\times\nabla T\right)\right]\\&=-\frac{5}{2e}\left[\nabla\times\left(\frac{nT}{B}\mathbf{b}\right)\cdot\nabla T-\frac{nT}{B}\mathbf{b}\cdot\cancelto{0}{(\nabla\times\nabla T)}\right]\\&=\frac{5}{2}\frac{T}{eB}\mathbf{b}\cdot\nabla n\times\nabla T+\frac{5}{2}\frac{nT}{e}\frac{2}{BR}\frac{\partial T}{\partial y}.\end{aligned} \tag{2.118}$$

This result yields that only $\mathbf{E}\times\mathbf{B}$-drift contributes to the advection, the rest is compression. Hence, energy equation (2.13) can be written as

$$\frac{3}{2}\left(\frac{\partial}{\partial t}+\frac{\mathbf{b}}{B_0}\times\nabla\phi\cdot\nabla\right)T+T\mathcal{K}(\phi)-\frac{7}{2}\frac{T}{e}\mathcal{K}(T)-\frac{T^2}{en}\mathcal{K}(n)=0, \tag{2.119}$$

$$\frac{3}{2}\frac{\partial T}{\partial t}+\frac{1}{B_0}\{\phi,T\}-\frac{2T}{B_0R_0}\frac{\partial\phi}{\partial y}+\frac{7}{2}\frac{T}{R_0B_0e}\frac{\partial T}{\partial y}+\frac{T^2}{enB_0R_0}\frac{\partial n}{\partial y}=0 \tag{2.120}$$

We will add a characteristic temperature $\mathcal{T}$ to the set of the dimensionless quantities (2.55). Let

$$T\to\hat{T}=\frac{T}{\mathcal{T}} \tag{2.121}$$

Then, the normalized continuity equation (2.110) is

$$\gamma\mathcal{N}\left(\frac{\partial\hat{n}}{\partial\hat{t}}+\{\hat{\phi},\hat{n}\}\right)-\frac{2l\gamma\mathcal{N}\hat{n}}{R_0}\frac{\partial\hat{\phi}}{\partial\hat{y}}+\frac{2}{e}\frac{\mathcal{N}\mathcal{T}\hat{n}}{B_0R_0l}\frac{\partial\hat{T}}{\partial\hat{y}}+\frac{2}{e}\frac{\mathcal{N}\mathcal{T}\hat{T}}{B_0R_0l}\frac{\partial\hat{n}}{\partial\hat{y}}=0, \tag{2.122}$$

$$\frac{\partial\hat{n}}{\partial\hat{t}}+\{\hat{\phi},\hat{n}\}-\frac{2l}{R_0}\hat{n}\frac{\partial\hat{\phi}}{\partial\hat{y}}+\frac{2}{e\gamma}\frac{\mathcal{T}}{B_0R_0l}\frac{\partial(\hat{T}\hat{n})}{\partial\hat{y}}=0. \tag{2.123}$$

We define the normalized vorticity as

$$\hat{\Omega}=\hat{\nabla}_\perp^2\hat{\phi} \tag{2.124}$$

and obtain normalized vorticity equation

$$\mathcal{N}\hat{n}\gamma^2B_0\left(\frac{\partial\hat{\Omega}}{\partial\hat{t}}+\{\hat{\phi},\hat{\Omega}\}\right)+\frac{2\mathcal{T}\hat{T}}{R_0m_i}\frac{\mathcal{N}}{l}\frac{\partial\hat{n}}{\partial\hat{y}}+\frac{2\mathcal{N}\hat{n}}{m_iR_0}\frac{\mathcal{T}}{l}\frac{\partial\hat{T}}{\partial\hat{y}}=0, \tag{2.125}$$

$$\hat{n}\left(\frac{\partial\hat{\Omega}}{\partial\hat{t}}+\{\hat{\phi},\hat{\Omega}\}\right)+\frac{2\mathcal{T}}{B_0\gamma^2R_0lm_i}\frac{\partial(\hat{n}\hat{T})}{\partial\hat{y}}=0 \tag{2.126}$$

$$\frac{\partial\hat{\Omega}}{\partial\hat{t}}+\{\hat{\phi},\hat{\Omega}\}+\frac{2\mathcal{T}}{B_0\gamma^2R_0lm_i}\left(\hat{T}\frac{\partial\ln\hat{n}}{\partial\hat{y}}+\frac{\partial\hat{T}}{\partial\hat{y}}\right)=0 \tag{2.127}$$

The normalized energy equation is

$$\mathcal{T}\gamma\left(\frac{\partial\hat{T}}{\partial\hat{t}}+\{\hat{\phi},\hat{T}\}\right)-\frac{2\mathcal{T}}{B_0R_0}\gamma B_0l\frac{\partial\hat{\phi}}{\partial\hat{y}}+\frac{7}{2}\frac{\mathcal{T}^2\hat{T}}{eR_0B_0l}\frac{\partial\hat{T}}{\partial\hat{y}}+\frac{\mathcal{T}^2\hat{T}^2}{eR_0B_0l\hat{n}}\frac{\partial\hat{n}}{\partial\hat{y}}=0, \tag{2.128}$$

$$\frac{\partial\hat{T}}{\partial\hat{t}}+\{\hat{\phi},\hat{T}\}-\frac{2l}{R_0}\frac{\partial\hat{\phi}}{\partial\hat{y}}+\frac{7}{2}\frac{\mathcal{T}\hat{T}}{e\gamma R_0B_0l}\frac{\partial\hat{T}}{\partial\hat{y}}+\frac{\mathcal{T}}{eR_0B_0l\gamma}\frac{\hat{T}^2}{\hat{n}}\frac{\partial\hat{n}}{\partial\hat{y}}=0. \tag{2.129}$$

We can also chose the characteristic frequency to be

$$\gamma=\frac{\mathcal{T}}{eB_0l^2} \tag{2.130}$$

and rewrite the normalized equations as

$$\frac{\partial \hat{n}}{\partial \hat{t}} + \{\hat{\phi}, \hat{n}\} - \frac{2l}{R_0}\hat{n}\frac{\partial \hat{\phi}}{\partial \hat{y}} + \frac{2l}{R_0}\frac{\partial(\hat{T}\hat{n})}{\partial \hat{y}} = 0, \tag{2.131}$$

$$\frac{\partial \hat{\Omega}}{\partial \hat{t}} + \{\hat{\phi}, \hat{\Omega}\} + \frac{2\mathcal{T}}{B_0\gamma^2 R_0 l m_i}\left(\hat{T}\frac{\partial \ln \hat{n}}{\partial \hat{y}} + \frac{\partial \hat{T}}{\partial \hat{y}}\right) = 0, \tag{2.132}$$

$$\frac{\partial \hat{T}}{\partial \hat{t}} + \{\hat{\phi}, \hat{T}\} - \frac{2l}{R_0}\frac{\partial \hat{\phi}}{\partial \hat{y}} + \frac{7}{2}\frac{2l\hat{T}}{R_0}\frac{\partial \hat{T}}{\partial \hat{y}} + \frac{l}{R_0}\frac{\hat{T}^2}{\hat{n}}\frac{\partial \hat{n}}{\partial \hat{y}} = 0. \tag{2.133}$$

We will analogously to (2.65) neglect the terms of order l/R_0 and therefore obtain the reduced three-field model equations, which are

$$\frac{\partial \ln \hat{n}}{\partial \hat{t}} + \{\hat{\phi}, \ln \hat{n}\} = 0, \tag{2.134}$$

$$\frac{\partial \hat{\Omega}}{\partial \hat{t}} + \{\hat{\phi}, \hat{\Omega}\} + \hat{T}\frac{\partial \ln \hat{n}}{\partial \hat{y}} + \frac{\partial \hat{T}}{\partial \hat{y}} = 0, \tag{2.135}$$

$$\frac{\partial \ln \hat{T}}{\partial \hat{t}} + \{\hat{\phi}, \ln \hat{T}\} = 0, \tag{2.136}$$

$$\hat{\Omega} = \hat{\nabla}_\perp^2 \hat{\phi}. \tag{2.137}$$

Taking isothermal limit, i.e. when $\hat{T} = 1$ we can reduce this model to the two-field model described by equations (2.66)-(2.67). Equation (2.136) describes the advection of the temperature with the electric drift. This model also has no free parameters, and the length scale of the blob is the only length scale in this model, so the density and the temperature have the same length scale. Assumption about non-isothermal ions is more natural in comparison with the isothermal case, therefore this model more precisely describes the filament motions is plasma and the results from the numerical simulations should better match the experimental results. If the density is constant, we obtain the model which is identical to the two-field model, where the temperature advection contributes to the filament motions in the same way as the density does.

For small density and temperature oscillations we can write model as

$$\frac{\partial \hat{n}'}{\partial \hat{t}} + \{\phi, \hat{n}'\} = 0, \tag{2.138}$$

$$\frac{\partial \hat{\Omega}}{\partial \hat{t}} + \{\hat{\phi}, \hat{\Omega}\} + \frac{\partial \hat{n}'}{\partial \hat{y}} + \frac{\partial \hat{T}'}{\partial \hat{y}} = 0, \tag{2.139}$$

$$\frac{\partial \hat{T}'}{\partial \hat{t}} + \{\hat{\phi}, \hat{T}'\} = 0. \tag{2.140}$$

This result yields that the density oscillations contributes as much as temperature does. It also means that the model with the isothermal electrons will be trivially identical to the one with the constant density.

2.6 Energy theorem for non-isothermal ions

To derive an energy theorem we will make the same assumptions that were described in chapter 2.3. We will also assume that the initial density and temperature are given by

$$\hat{n} = 1 + \frac{\Delta n}{\mathcal{N}} n', \tag{2.141}$$

$$\hat{T} = 1 + \frac{\Delta T}{\mathcal{T}} T', \tag{2.142}$$

where $\frac{\Delta T}{\mathcal{T}} \ll 1$ and $\frac{\Delta n}{\mathcal{N}} \ll 1$.

We redefine the potential energy as

$$\hat{E}_p = \int \mathrm{d}\hat{A}\, \hat{x}(\hat{n}' + \hat{T}'). \tag{2.143}$$

Hence, to obtain an energy equation we add equation (2.134) to equation (2.136) and multiply them with $\int \mathrm{d}\hat{A}\, x$, obtaining

$$\int \mathrm{d}\hat{A}\, \hat{x} \left(\frac{\partial(\hat{n} + \hat{T})}{\partial \hat{t}} \right) + \int \mathrm{d}\hat{A}\, \hat{x}(\{\hat{\phi}, \hat{n}\} + \{\hat{\phi}, \hat{T}\}) = 0. \tag{2.144}$$

The second term of (2.144) is

$$\int \mathrm{d}\hat{A}\, (\hat{n}' + \hat{T}') \frac{\partial \hat{\phi}}{\partial \hat{y}} = -\int \mathrm{d}\hat{A}\, (\hat{n}' + \hat{T}') v_x \equiv -\Gamma_n, \tag{2.145}$$

where $\Gamma_{\hat{n}}$ denotes the particle flux. Therefore, we can rewrite (2.144) as

$$\frac{\mathrm{d}\hat{E}_k}{\mathrm{d}\hat{t}} = -\Gamma_{\hat{n}}. \tag{2.146}$$

Since only small temperature and density amplitude oscillations are considered, we again define the kinetic energy as

$$\hat{E}_k = \int \mathrm{d}\hat{A}\, (\hat{\nabla}\hat{\phi})^2. \tag{2.147}$$

We multiply the vorticity equation (2.135) by $\int \mathrm{d}\hat{A}\, \hat{\phi}$ and obtain

$$\int \mathrm{d}\hat{A}\, \hat{\phi} \frac{\partial \hat{\nabla}_\perp^2 \hat{\phi}}{\partial \hat{t}} + \int \mathrm{d}\hat{A}\, \hat{\phi} \{\hat{\phi}, \hat{\nabla}_\perp^2 \hat{\phi}\} + \int \mathrm{d}\hat{A}\, \hat{\phi} \frac{\partial \hat{n}'}{\partial \hat{y}} + \int \mathrm{d}\hat{A}\, \hat{\phi} \frac{\partial \hat{T}'}{\partial \hat{y}} = 0. \tag{2.148}$$

using results (2.83) - (2.85), we can rewrite (2.148) as

$$\frac{\mathrm{d}\hat{E}}{\mathrm{d}\hat{t}} = \Gamma_{\hat{n}}. \tag{2.149}$$

Thus, adding (2.149) to (2.146) we derive an energy theorem for small density and temperature oscillations is

$$\frac{\mathrm{d}}{\mathrm{d}\hat{t}}(\hat{E}_p + \hat{E}_k) = 0. \tag{2.150}$$

This results yields that the sum of the potential and the kinetic energy is a conserved quantity. Taking isothermal limit $\hat{T} = 1$ we arrive at (2.94), which means that in case of the non-isothermal electrons we extend the definition of the potential and the kinetic energy, and the temperature oscillations contribute to the energy dynamics in the same way as density oscillations do. The interchange of the energy in the model happens through the flux of the particles.

2.7 Velocity scaling laws for non-isothermal electrons

Analogously to the density model (2.70) we will assume that the temperature is also given as a sum of the constant background temperature and the oscillating part

$$\hat{T} = 1 + \frac{\Delta T}{\hat{T}} T', \tag{2.151}$$

where ΔT is an oscillation amplitude.

If we assume constant temperature, velocity scaling is

$$\hat{V} \sim \left(\frac{\Delta n}{\mathcal{N}}\right)^{1/2}. \tag{2.152}$$

for small oscillation amplitudes, and

$$\hat{V} \sim 1. \tag{2.153}$$

for large oscillation amplitudes. If we instead assume constant density, i.e. $\hat{n} = 1$ model equations reduce to

$$\frac{\mathrm{d}\hat{\Omega}}{\mathrm{d}\hat{t}} + \frac{\partial \hat{T}}{\partial \hat{y}} = 0, \tag{2.154}$$

$$\frac{\partial \ln \hat{T}}{\partial \hat{t}} + \{\hat{\phi}, \ln \hat{T}\} = 0. \tag{2.155}$$

Analogously to (2.99)-(2.106) we derive the velocity scaling law, which in non-dimensional units is given by

$$\hat{V} \sim \left(\frac{\Delta T}{\mathcal{T}}\right)^{1/2}, \tag{2.156}$$

and in dimensional units is

$$\frac{V}{C_s} \sim \left(\frac{2l}{R_0}\frac{\Delta T}{\mathcal{T}}\right)^{1/2}. \tag{2.157}$$

It yields that the velocity V scales as a square root of the amplitude $\Delta T/\mathcal{T}$ independently on the size of the amplitude, because last term of (2.135) is not logarithmic. This is also the only allowable scaling according to the dimensional analysis, because there are no free parameters in this model. These analytic results will hold for the limits $\frac{|\Delta T|}{\mathcal{T}} \ll \frac{|\Delta n|}{\mathcal{N}}$ and $\frac{|\Delta n|}{\mathcal{N}} \ll \frac{|\Delta T|}{\mathcal{T}}$, but when the temperature and density oscillations are of the same order, velocity scaling laws can only be derived numerically.

3

Numerical methods and code testing

In this chapter we describe numerical methods that were used to solve the model equations and provide several results for isolated blob simulations.

The model equations that were derived in the previous chapter are known to be the convection-diffusion equations of the form

$$\frac{\partial v}{\partial t} = \mathcal{L}_v(n, \Omega, \phi, T) - (\mathbf{u} \cdot \nabla)v + \mu_{D,v}\nabla_\perp^2 v - \mu_H \nabla_\perp^4 v, \quad u = n, \Omega, T, \quad (3.1)$$

where $\mathcal{L}_v$ is a linear differential operator, $\mu_{D,v}$ is a diffusion coefficient, μ_H is a hyperviscous diffusion coefficient. With certain assumptions and approximations we can solve these equations by finite difference and spectral differentiation methods.

3.1 Finite difference

We consider a rectangular simulation domain of the size $(-\frac{L_x}{2}, \frac{L_x}{2}) \times (-\frac{L_y}{2}, \frac{L_y}{2})$ and introduce a cell-centered grid with N equidistant points in x-direction and M equidistant points in y-direction, such that their position is given by

$$x_n = -L_x + (n + \frac{1}{2})dx, \quad n = 0, \ldots, N-1, \tag{3.2}$$

$$y_n = -L_y + (n + \frac{1}{2})dy, \quad n = 0, \ldots, M-1, \tag{3.3}$$

where $dx = L_x/N$, $dy = L_y/M$. Finite-difference methods solve differential

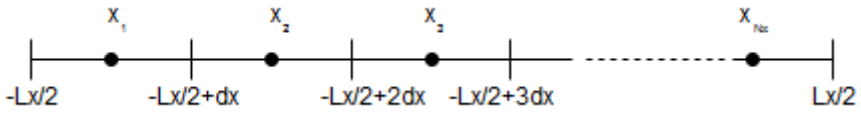

Figure 3.1: Cell-centered grid.

equations by approximating them with the difference equations, in which finite differences approximate the derivatives. The difference equations for first and second order derivatives are given by

$$\frac{\partial v}{\partial x}(x_n) = \frac{1}{2dx}(v_{n+1} - v_{n-1}) + O(dx^2), \tag{3.4}$$

$$\frac{\partial^2 v}{\partial x^2}(x_n) = \frac{1}{dx^2}(v_{n-1} - 2v_n + v_{n+1}) + O(dx^2) \tag{3.5}$$

If we assume Dirichlet boundary conditions, i.e. when the values of v are specified at the boundaries, then we need to introduce ghost points v_0 and v_{N+1}. These points are not elements of the given set of grid points, but they allow us to solve difference equations (3.4) and (3.5) [21]. Using linear extrapolation across the boundary of the domain we can relate the values of the domain boundaries to the value at the cell centers by

$$V_{\frac{1}{2}} = \frac{1}{2}(v_0 + v_1) + O(dx^2), \tag{3.6}$$

$$V_{N+\frac{1}{2}} = \frac{1}{2}(v_N + v_{N+1}) + O(dx^2). \tag{3.7}$$

Using these equations we can calculate the values of v at the ghost points

$$v_0 = 2V_{\frac{1}{2}} - v_1 + O(dx^2), \tag{3.8}$$

$$v_{N+1} = 2V_{\frac{1}{2}} - v_N + O(dx^2) \tag{3.9}$$

and solve difference equations (3.4), (3.5).

3.2 Spectral transformations and spectral differentiation

We consider a periodic function $v(x)$, i.e. $v(x) = v(x+T)$. We are also sampling this function into N numbers such that $v_m = v(x_m)$ and $x_m = m \cdot dy$,for $m = 0, 1, \ldots, M_y - 1$. The discrete Fourier transform transforms sequence v_m into into another sequence of complex numbers, $\hat{v}_0, \hat{v}_1, \ldots, \hat{v}_{N-1}$ which is defined by

$$\hat{v}_m = \sum_{n=0}^{M-1} v_n e^{2\pi \frac{inm}{M}}, \quad m = 0, \ldots, M-1 \tag{3.10}$$

The Inverse Discrete Fourier Transform (IDFT) is defined by

$$v_m = \frac{1}{M} \sum_{n=0}^{m-1} \hat{v}_n e^{-\frac{2\pi imn}{M}}, \quad m = 0, \ldots, M-1. \tag{3.11}$$

The first and the second derivatives of u can now be calculated via DFT:

$$v'_m = v\left(\frac{mL_y}{M}\right) = \frac{1}{M} \sum_{m=0}^{M_y-1} \hat{u}'_m e^{-\frac{2\pi inm}{M}}, \tag{3.12}$$

$$v''_m = v\left(\frac{mL_y}{M}\right) = \frac{1}{M} \sum_{m=0}^{M-1} \hat{u}''_m e^{-\frac{2\pi inm}{M}}. \tag{3.13}$$

This scheme uses vertically centered grid which is defined as

$$x_n = -Lx + dx \cdot n, \quad n = 0, \ldots, N-1 \tag{3.14}$$

and is shown on Figure (3.4). We can apply spectral transformations to the pe-

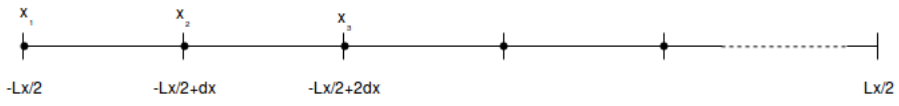

Figure 3.2: Vertically centered grid.

riodic boundary conditions, i.e. for $v(-L/2) = v(L/2)$, perform differentiation in the Fourier space and then transform the function back. The definition of (3.10) requires $O(N^2)$ operations since there are N outputs of X_m, and each output requires a sum of N terms. However, the calculation speed of DFT can be increased if we apply so-called Fast Fourier Transform method which reduces the number of operations to $O(N \log N)$ and makes working with the Discrete Fourier Transforms reasonable [22].

3.3 Time integration scheme

For time integration we use $K-th$ order stable integration, presented in [**?**], which is used in the *2dads*-code [23]. If we neglect the hyperviscous term and the advective derivative, diffusion equation (3.1) can be generalized as

$$\frac{\partial v}{\partial t} = \mu_D \frac{\partial^2 v}{\partial x^2} + \mathcal{L}v \tag{3.15}$$

The stable integration scheme is given by

$$\frac{1}{dt}\left(a_0 v^i - \sum_{k=1}^{K} v_{i-k}\right) = \kappa\delta_x^2 + \sum_{k=1}^{K} \beta_k \mathcal{L}v^{i-k} + O(dt^K), \tag{3.16}$$

where δ_x^2 is the discretisation of the second order spatial derivative, and coefficients α and β are specified in such way that they provide $k-th$ order accuracy. The more detailed information about their values and this scheme can be found at [24]. We can rearrange equation (3.16) as

$$-r_x v_{n-1}^i + (\alpha_0 + 2r_x)v_n^i - r_x u_{n+1}^i = \sum_{k=1}^{K} (\alpha_k v_n^{i-k} + dt\beta_k \mathcal{L}v_n^{i-k} + O(dt_t^K + dx^2), \tag{3.17}$$

where $r_x = kdt/dx^2$. In case of Dirichlet boundary conditions we use the following scheme

$$(\alpha_0 + 3r_x)v_1^i - r_x v_2^i = \sum_{k=1}^{K} (\alpha_k v_1^{i-k} + \beta_k \mathcal{L}v_1^{i-k}) + 2r_x V_{1/2}, \tag{3.18}$$

$$-r_x v_{N-1}^i + (\alpha_0 + 3r_x)v_n^i = \sum_{k=1}^{K} (\alpha_k v_N^{i-k} + \beta_k \mathcal{L}v_N^{i-k}) + 2r_x V_{N+1/2}. \tag{3.19}$$

3.4 Code testing

3.4.1 Simple diffusion equation

In order to verify code implementation we compare the numerical solution of the diffusion equation with the exact solution. Simple diffusion equation is given by

$$\frac{\partial n}{\partial t} = \kappa \nabla_{\perp}^2 n. \tag{3.20}$$

First we assume Dirichlet boundary conditions, i.e.

$$n(-L_x/2, 0, 0) = n(L_x/2, 0, 0) = 0, \quad n(0, -L_y/2, 0) = n(0, L_y/2, 0) = 0, \tag{3.21}$$

with the initial condition

$$n(\mathbf{x}, t) = \exp\left(-\frac{1}{2}\mathbf{x}^2\right). \tag{3.22}$$

If we chose $L_x = 20$, then at the boundary $n(5, 0, 0) \approx 0$. This result indicates that we can use finite the difference method for relatively large domains to solve problems with the Dirichlet boundary conditions. The exact solution of this equation is given by

$$n(\mathbf{x}, t) = \sum_{m=1}^{\infty} \sum_{n=1}^{\infty} A_{mn} \sin(\mu_m x) \sin(\nu_n y) \exp(-\lambda_{mn}^2 t), \tag{3.23}$$

where

$$\mu_m = \frac{m\pi}{L_x}, \quad \nu_n = \frac{n\pi}{L_y}, \quad \lambda_{mn} = \kappa\sqrt{\mu_m^2 + \nu_n^2},$$
$$A_{mn} = \frac{4}{L_x L_y} \int_{-L_x/2}^{L_x/2} \int_{-L_y/2}^{L_y/2} \mathrm{d}x\mathrm{d}y \; \exp\left(-\frac{x^2 + y^2}{2}\right) \sin\left(\frac{m\pi}{L_x}x\right) \sin\left(\frac{m\pi}{L_y}y\right). \tag{3.24}$$

We vary number of grid points and expect that error will decrease when number of grid points increases.

If the periodic boundary conditions are assumed with the same initial condition (3.22), the solution to (3.20) is given by

$$n(\mathbf{x}, t) = \sum_{m=0}^{\infty} \sum_{n=0}^{\infty} A_{mn} \cos(\mu_n x) \cos(\mu_m y) \exp(-\kappa \lambda_{mn} t) \tag{3.25}$$

where

$$\mu_m = \frac{m\pi}{L_x}, \quad \nu_n = \frac{n\pi}{L_y}, \quad \lambda_{mn} = \kappa\sqrt{\mu_m^2 + \nu_n^2},$$
$$A_{00} = \frac{1}{4L_xL_y}\int_{-L_x/2}^{L_x/2}\int_{-L_y/2}^{L_y/2} \mathrm{d}x\mathrm{d}y \;\; \exp\left(-\frac{x^2+y^2}{2}\right)$$
$$A_{mn} = \int_{-L_x/2}^{L_x/2}\int_{-L_y/2}^{L_y/2} \mathrm{d}x\mathrm{d}y \;\; \exp\left(-\frac{x^2+y^2}{2}\right)\cos(\mu_m x)\cos(\nu_n y) \tag{3.26}$$

We compare the exact solution with the numerical and note that the conver-

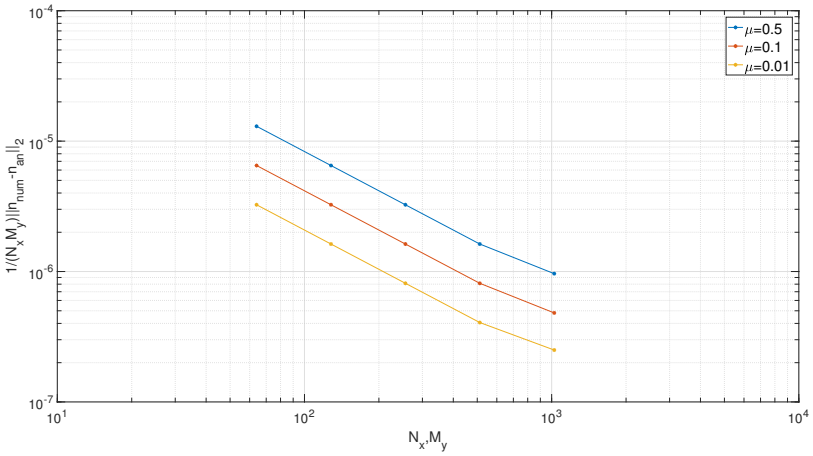

Figure 3.3: Convergence rate of the error of the finite difference method solving simple diffusion equation (3.20) with 4th order time integration.

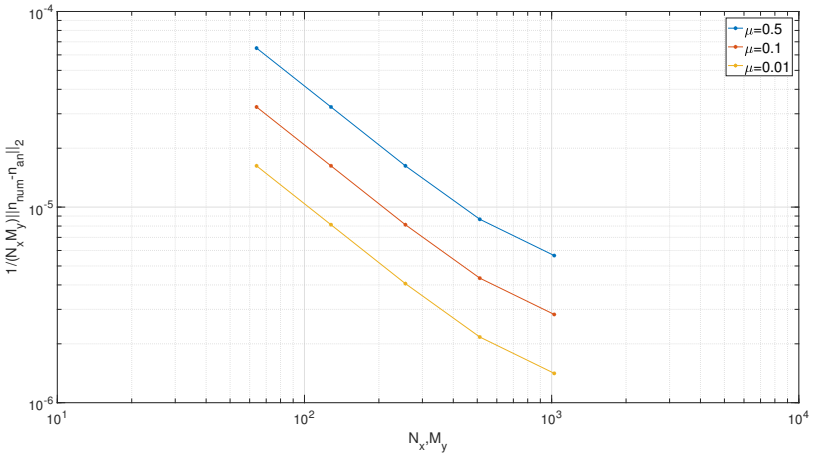

Figure 3.4: Convergence rate of the error of the spectral differentiation method solving simple diffusion equation with periodic boundary conditions (3.20) with 4th order time integration.

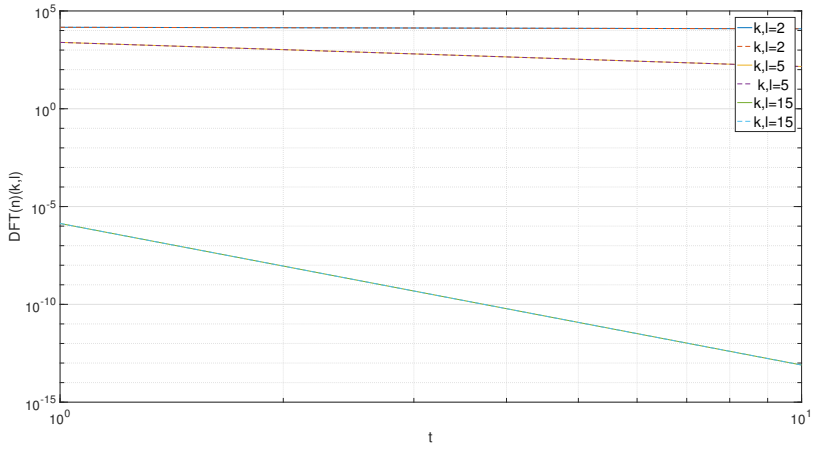

Figure 3.5: Convergence rate of the different Fourier modes of the exact and numerical (dotted lines) solutions of (3.20) for $\mu = 0.1$.

gence rate flatterns out due to the error of the time derivative witch does not change for different resolutions. To make sure that the error of the spectral differentiation method does not happen due to aliasing we also check the convergence of the Fourier modes with respect to the time. The result is shown on Figure 3.5.

These results yield that both schemes can be successfully used to solve model equations.

3.5 Simple blob simulations and convergence tests

We can solve the three-field model equations (2.134)-(2.137) as diffusion equations numerically by balancing them with the advection and neglecting hyperviscous terms.

$$\frac{\partial \hat{n}}{\partial \hat{t}} + \{\hat{\phi}, \hat{n}\} = \mu \hat{\nabla}_{\perp}^2 \hat{n}, \tag{3.27}$$

$$\frac{\partial \hat{\Omega}}{\partial \hat{t}} + \{\hat{\phi}, \hat{\Omega}\} + \hat{T}\frac{\partial \ln \hat{n}}{\partial \hat{y}} + \frac{\partial \hat{T}}{\partial \hat{y}} = \kappa \hat{\nabla}_{\perp}^2 \hat{\Omega}, \tag{3.28}$$

$$\frac{\partial \hat{T}}{\partial \hat{t}} + \{\hat{\phi}, \hat{T}\} = \chi \hat{\nabla}_{\perp}^2 \hat{T}, \tag{3.29}$$

$$\hat{\Omega} = \hat{\nabla}_{\perp}^2 \hat{\phi}. \tag{3.30}$$

where μ is a nondimensional dissipation coefficient of the density, κ is a nondimensional dissipation coefficient of the vorticity and χ is a nondimensional dissipation coefficient of the temperature. Logarithmic derivative is given by

$$\hat{\nabla}_\perp \ln \hat{n} = \frac{\hat{\nabla}_\perp \hat{n}}{\hat{n}}. \tag{3.31}$$

Hence, we can rewrite equation (3.27) as

$$\frac{\partial \hat{n}}{\partial \hat{t}} + \{\phi, \hat{n}\} = \mu \hat{\nabla}_\perp \cdot (\hat{n} \hat{\nabla}_\perp \ln \hat{n}), \tag{3.32}$$

and, using a rule for the divergence of a scalar and a vector, we get

$$\frac{\partial \hat{n}}{\partial \hat{t}} + \{\phi, \hat{n}\} = \mu \hat{n} \hat{\nabla}_\perp^2 \ln \hat{n} + \mu \hat{\nabla}_\perp \hat{n} \hat{\nabla}_\perp \ln \hat{n}. \tag{3.33}$$

Since density $\hat{n}$ is always a positive quantity, we divide both parts by $\hat{n}$ and obtain the logarithmic formulation of the continuity equation

$$\frac{\partial \ln \hat{n}}{\partial \hat{t}} + \{\phi, \ln \hat{n}\} = \mu \nabla_\perp^2 \ln \hat{n} + \mu (\nabla_\perp \ln \hat{n})^2. \tag{3.34}$$

Hence, the model equations (3.27)-(3.30) can be written as

$$\frac{\partial \ln \hat{n}}{\partial \hat{t}} + \{\hat{\phi}, \ln \hat{n}\} = \mu \nabla_\perp^2 \ln \hat{n} + \mu (\nabla_\perp \ln \hat{n})^2, \tag{3.35}$$

$$\frac{\partial \hat{\Omega}}{\partial \hat{t}} + \{\hat{\phi}, \hat{\Omega}\} + \hat{T} \frac{\partial \ln \hat{n}}{\partial \hat{y}} + \frac{\partial \hat{T}}{\partial \hat{y}} = \kappa \hat{\nabla}_\perp^2 \hat{\Omega}, \tag{3.36}$$

$$\frac{\partial \ln \hat{T}}{\partial \hat{t}} + \{\hat{\phi}, \ln \hat{T}\} = \chi \nabla_\perp^2 \ln \hat{T} + \chi (\nabla_\perp \ln \hat{T})^2, \tag{3.37}$$

$$\hat{\Omega} = \hat{\nabla}_\perp^2 \hat{\phi}. \tag{3.38}$$

Further in this study we will assume that the initial density and the initial temperature are given by

$$\hat{n} = 1 + \frac{\Delta n}{\mathcal{N}} \exp\left(-\frac{\mathbf{x}^2}{2}\right), \tag{3.39}$$

$$\hat{T} = 1 + \frac{\Delta T}{\mathcal{T}} \exp\left(-\frac{\mathbf{x}^2}{2}\right). \tag{3.40}$$

This model now has five paramters, which are μ, κ, χ, $\Delta n/\mathcal{N}$ and $\Delta T/\mathcal{T}$. In order to reduce the number of the parameters and to study how the dissipation coefficients affect this model we perform the new normalization. We consider an isothermal case. Let

$$\hat{\gamma} \to \tilde{\gamma} = \hat{\gamma} (\Delta n/\mathcal{N})^{1/2}, \ \hat{\phi} \to \tilde{\phi} = \frac{\hat{\phi}}{(\Delta n/\mathcal{N})}, \ \hat{\Omega} \to \tilde{\Omega} = \frac{\hat{\Omega}}{(\Delta n/\mathcal{N})} \tag{3.41}$$

Then model can be written as

$$\frac{\partial \tilde{n}}{\partial \tilde{t}} + \{\tilde{\phi}, \tilde{n}\} = \tilde{\kappa}\hat{\nabla}_{\perp}^{2}\tilde{n}, \tag{3.42}$$

$$\frac{\partial \tilde{\Omega}}{\partial \tilde{t}} + \{\tilde{\phi}, \tilde{\Omega}\} + \frac{\partial \tilde{n}}{\partial \tilde{y}} = \tilde{\mu}\hat{\nabla}_{\perp}^{2}\tilde{\Omega} \tag{3.43}$$

with the initial condition

$$\tilde{n}(\hat{t} = 0) = \exp\left(-\frac{\mathbf{x}^2}{2}\right), \tag{3.44}$$

where we define dissipation coefficients as

$$\tilde{\mu} = \mu/(\Delta n/\mathcal{N})\,, \tilde{\kappa} = \kappa/(\Delta n/\mathcal{N})\,. \tag{3.45}$$

In comparison with (3.35)-(3.38), model (3.42)-(3.42) has only two parameters and is identical to the one decribing two-dimensional thermal convection in a thin fluid layer. It should be also noted that we can assume constant density and non-isothermal electrons and replace $\tilde{n}$ by $\tilde{T}$, so the further results will be trivially valid for the temperature equation, when the constant density is assumed. We identify the corresponding Rayleigh and Prandtl numbers as

$$\mathrm{Ra} = \frac{1}{\tilde{\kappa}\tilde{\mu}}, \quad \mathrm{Pr} = \frac{\tilde{\mu}}{\tilde{\kappa}}. \tag{3.46}$$

In fluid mechanics Rayleigh number is a dimensionless term used in the calculation of natural convection which identifies whether the heat transfer happens through the conduction or through the convection, it is the ratio of the effective buoyancy to the dissipative forces. The Prandtl number, is a dimensionless parameter representing the ratio of the diffusion of momentum to the diffusion of heat in a fluid. It measures the relative strength of viscosity and diffusion.

In order to investigate the dynamics of these blob structures, periodic boundary conditions are invoked for the drift plane perpendicular to the magnetic field. It yields that the integral

$$N = \int \mathrm{d}\hat{A}\,\hat{n} \tag{3.47}$$

is a conserved quantity. A quantitative description of the motion of the blob structure is given by the center-of-mass coordinates which are defined as

$$\hat{X}_c = \frac{1}{N}\int \mathrm{d}\hat{A}\hat{x}\hat{n}, \qquad \hat{Y}_c = \frac{1}{N}\int \mathrm{d}A\hat{y}\hat{n}. \tag{3.48}$$

We can therefore define center-of-mass velocity components as

$$\hat{V}_{\hat{x}} = \frac{\mathrm{d}X_c}{\mathrm{d}\hat{t}}, \qquad \hat{V}_{\hat{y}} = \frac{\mathrm{d}Y_c}{\mathrm{d}\hat{t}} \tag{3.49}$$

which can be easily calculated numerically. The integrals (3.47)-(3.48) will also be valid for normalized quantities (3.41).

We initialize model (3.42)-(3.43) for Pr= 1, Ra $= 10^6$ and compare the results with our theoretical expectations and previously published works. An isolated blob structure initially has neither electric potential, norvorticity, and the density has a symmetric structure. It accelerates and advects radially outwards, exactly as the energy theorem was predicting, along positive $\hat{x}$-direction and form the electric potential and the vorticity fields. The initial evolution is characterized by the formation of the front, across which the density varies sharply [15]. This front is followed by a trailing wake, and the density amplitude decays gradually. We can also see that the density develops into the shape of the mash room-like cap, this structure is well known for scalar fields subject to the interchange motions. The blob structure rolls up to in two lobes. Due to stretching and collisional diffusion, the leading front gradually disappears, leaving two disjonit entities. Each of these entities contains a net vorticity of the opposite polarity, shown on Figure 3.8. It is also important to note that in the flont line of the vorticity field, in the regions lying closely to $\hat{y} = 0$ vorticity equals zero, and this region may be identified as a gap. Reason to that is that the temporal change of the vorticity is balanced by the spatial change of the density, so vorticity cannot be generated there.

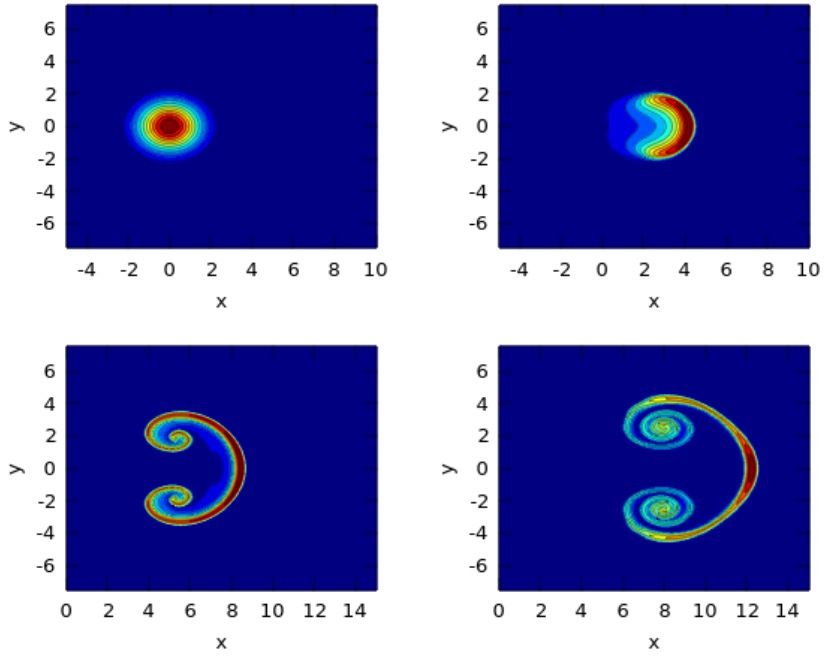

Figure 3.6: Evolution of an isolated blob structure for Ra$=10^6$ and Pr$=1$, showing the density $\tilde{n}$ at time $\hat{t}=0$ at the top left corner, increments every 5 time units.

In the previous publications [15], [25] it was mentioned that the particular care has to be taken about the size of the simulation domain and the grid resolution. We will therefore analyze how this parameters affect the model and find the optimal size of the simulation domain and number of the grid points. Figure 3.9 shows how different resolutions and domain lengths afffect the velocity.

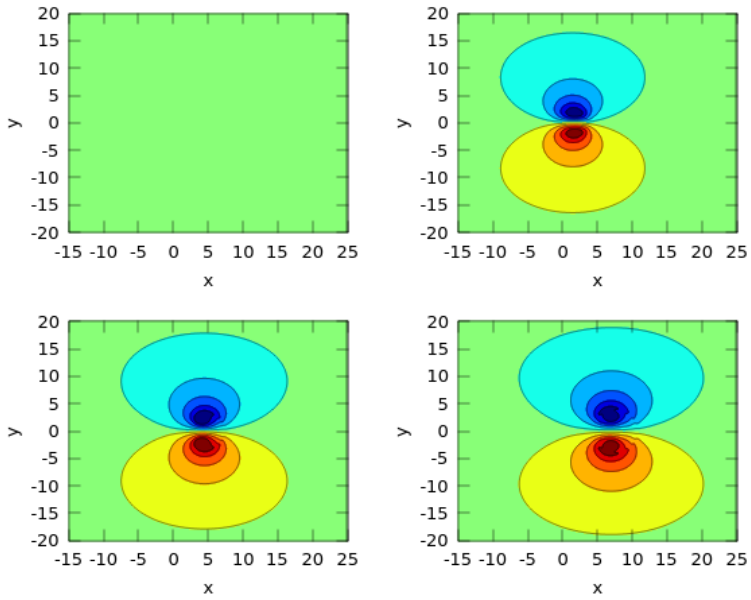

Figure 3.7: Evolution of an isolated blob structure for Ra= 10^6 and Pr= 1, showing the electric potential $\tilde{\phi}$ at time $\hat{t} = 0$ at the top left corner, increments every 5 time units.

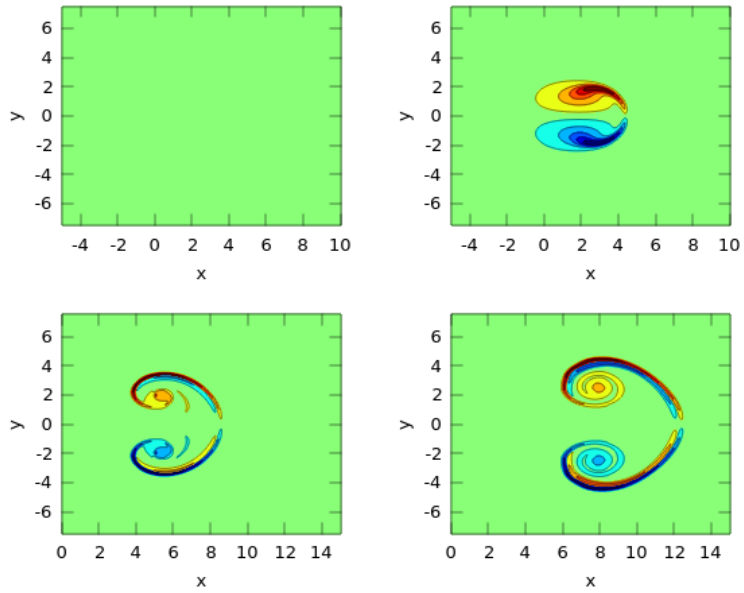

Figure 3.8: Evolution of an isolated blob structure for Ra= 10^6 and Pr= 1, showing the vorticity $\tilde{\Omega}$ at time $\hat{t} = 0$ at the top left corner, increments every 5 time units.

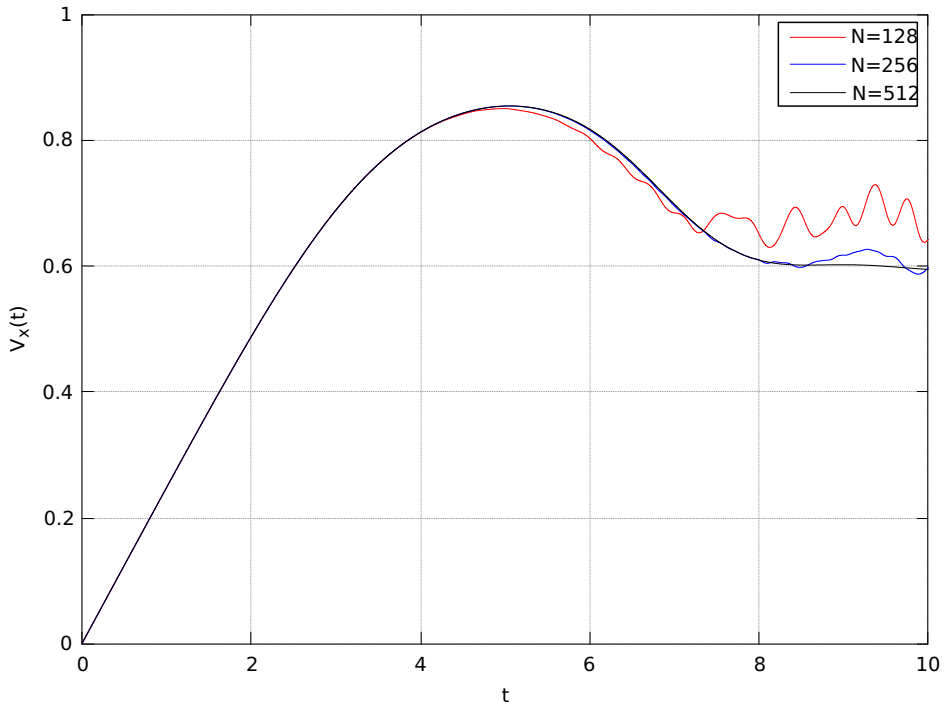

Figure 3.9: Temporal evolution of the center-of-mass velocity V_x for different grid resolutions

From Figure 3.9 we can see that if the grid size is chosen to be $N = 512$ and $L = 50$, we can estimate the maximum centre-of-mass velocity and analyze blob dynamics with the relatively high confidence. Further increase of the size of the simulation domain seems to be unreasonable and can affect the values of the integrals (3.47). The corresponding increase of the resolution that could compensate that increase would only increase the computational cost, while the results would be the same. From Figure 3.7 we can see that it is enough to choose the grid size to be $L = 50$, such that the filament is not affected by the boundaries and we can choose the grid resolution $N = 1024$.

Further we study how the variation of the Rayleigh numbers affects centre-of-mass velocity, when Prandtl number is assumed to be Pr$= 1$. Our goal is to find an optimal regime, where the velocity becomes independent on the collisional dissipation.
The results of the implementation of the model (3.42)-(3.43) for different Rayleigh numbers are pretested on the Figure 3.10. From this figure we can see that the maximum velocity becomes independent of the collisional dissipation when the Rayleigh number Ra $> 10^4$. In this case the maximum velocity transitions to the ideal regime where it remains constant. This result allows us to find the optimal values of the dissipation coefficients μ, κ and χ in the

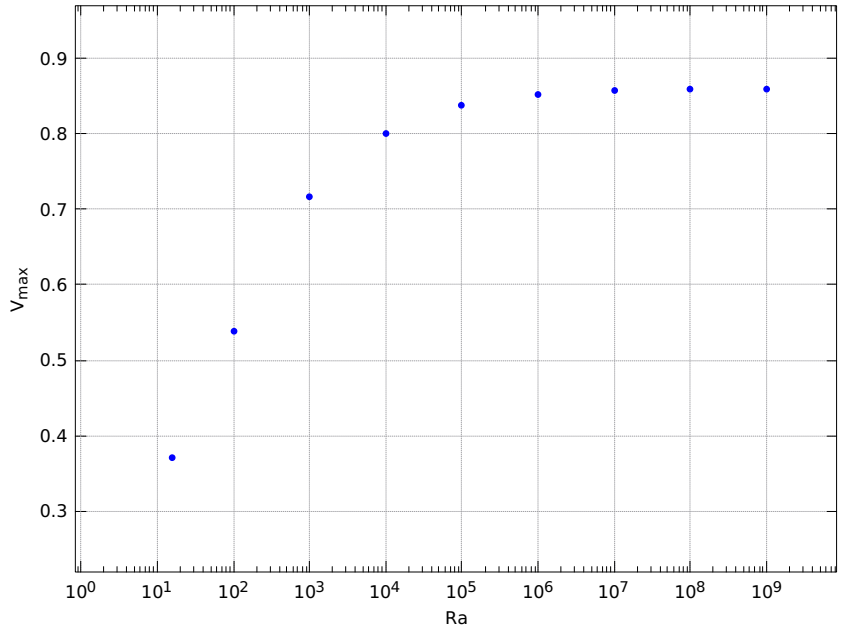

Figure 3.10: Maximal radial center-of-mass velocity of localized structures as function of the Rayleigh number for unit Prandtl number.

model (3.35)-(3.38), and proceed to the verification of the velocity scaling laws, where density and temperature amplitudes are the only parameters that we will vary.

3.6 Numerical verification of the velocity scaling laws

We assume that the initial electric potential, density and the temperature are given by

$$\hat{\phi}(\hat{t}=0)=0, \quad \hat{\Omega}(\hat{t}=0)=0, \tag{3.50}$$

$$\hat{n}(\hat{t}=0)=1+\frac{\Delta n}{\mathcal{N}}\exp\left(-\frac{\mathbf{x}^2}{2}\right), \tag{3.51}$$

$$\hat{T}(\hat{t}=0)=1+\frac{\Delta T}{\mathcal{T}}\exp\left(-\frac{\mathbf{x}^2}{2}\right). \tag{3.52}$$

In order to verify the velocity scaling laws we vary the density and temperature amplitudes in three different regimes. In the first regime isothermal electrons were assumed, in the second regime constant density was assumed and in

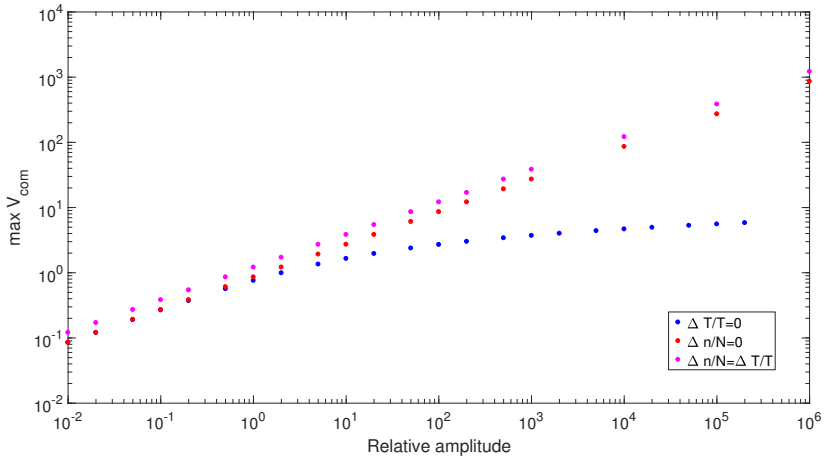

Figure 3.11: Maximal centre of mass velocity as a function of the density and temperature amplitude.

the third regime density oscillation amplitude was assume to be equal to the temperature oscillation amplitude. It should be noted that if we have equal density and temperature amplitudes, then there will be the dynamics for these variables, and center-of-mass velocity will be equal to the center-of-heat velocity. We vary amplitudes $\Delta n/\mathcal{N}$ and $\Delta T/\mathcal{T}$ from 10^{-2} to 10^{6}. The results of these numerical simulations are presented on the Figure 3.11.

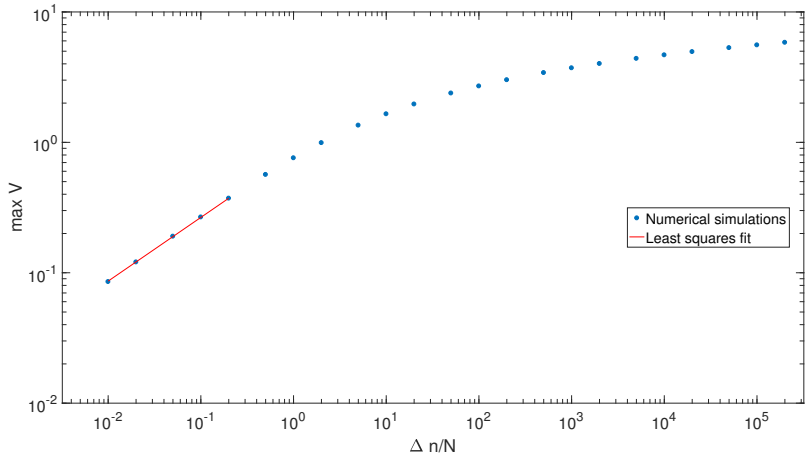

Figure 3.12: Maximal centre of mass velocity as a function of the density amplitude.

In order to verify the velocity scaling law for the small amplitudes we fit a two-term power series model with 95% confidence bounds for $\Delta n/\mathcal{N} < 1$, shown as a red line on the Figure 3.12. The model is

$$f(\Delta n/\mathcal{N}) = (0.818 \pm 0.010)(\Delta n/\mathcal{N})^{0.496\pm0.007}. \tag{3.53}$$

This result provides a confident agreement with the velocity scaling law for small amplitude. We can also see that for large amplitudes velocity flatterns, and the dependence there is very weak. However, the velocity is not seen to become completely independent of the amplitude, From the velocity scaling law for large density amplitudes (2.106) we expected that velocity would become completely independent on the density amplitude, but there still exists a weak dependence. This happens most likely due to the more sustainable blob-like structure during the filament motion which keeps the dipole vorticity generation and, thereby, larger radial velocities compared to the low amplitude case [25].

When the constant density is assumed, the velocity scaling will be valid for all temperature amplitudes. We analogously to (3.53) fit a two-term power series model with 95% confidence bounds, which is

$$f(\Delta T/\mathcal{T}) = (0.8617 \pm 0.0004)\,(\Delta T/\mathcal{T})^{0.4998\pm0.0001}\,. \tag{3.54}$$

This result provides an excellent agreement with the velocity scaling law (2.156) that showed that in this regime the scaling is independent of the temperature amplitude.

We have discussed that when the density and temperature amplitudes are equal, the velocity scaling law can only be derived numerically. First we try

model fitting to the whole domain of the amplitudes. This yields

$$f(\Delta T/\mathcal{T}) = (1.214 \pm 0.020)\,(\Delta T/\mathcal{T})^{0.5022\pm0.0022}\,. \tag{3.55}$$

However, for small amplitudes we expect that the density and the temperature will have the same contribution, so we expect the velocity scaling law to be of the form:

$$\hat{V} \sim \left(\frac{\Delta n}{\mathcal{N}} + \frac{\Delta T}{\mathcal{T}}\right)^{1/2}, \tag{3.56}$$

which in case of equal amplitudes yields

$$\hat{V} \sim \left(2\frac{\Delta n}{\mathcal{N}}\right)^{1/2}. \tag{3.57}$$

For the large amplitudes density will not contribute to the scaling, and the scaling law becomes

$$\hat{V} \sim \left(\frac{\Delta T}{\mathcal{T}}\right)^{1/2}. \tag{3.58}$$

Therefore we can obtain more precise results by fitting the model to the two

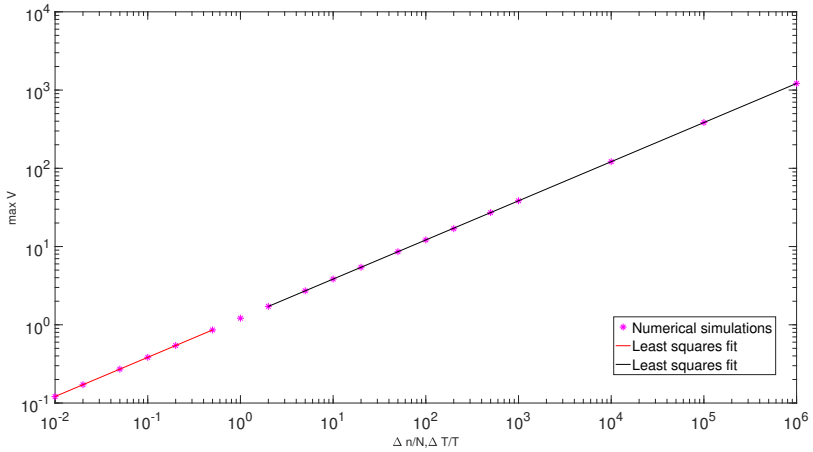

Figure 3.13: Maximal centre of mass velocity as a function of the density and temperature amplitude.

different amplitude ranges. Thus, for $\Delta n/\mathcal{N} < 1$ we obtain

$$f(\Delta T/\mathcal{T}) = (1.2160 \pm 0.0005)(\Delta T/\mathcal{T})^{0.5006\pm0.0003}, \tag{3.59}$$

shown as the red line on Figure 3.13, and for $\Delta n/\mathcal{N} > 1$ we get

$$f(\Delta T/\mathcal{T}) = (1.214 \pm 0.003)(\Delta T/\mathcal{T})^{0.5001\pm0.0002}, \tag{3.60}$$

where this fit shown as black line on a Figure 3.13. We note that the models (3.59) and (3.60) have smaller confidence bounds than (3.55), and therefore more precisely describe the scaling laws. Larger confidence interval of the estimate of the proportionality factor in (3.60) can be explained by the same reasons that we mentioned for the isothermal model. We can therefore conclude that all the velocity scaling laws that were derived here are correct, and we can continue to study this model by making more complicated assumptions about the temperature and density amplitudes.

4

Conclsuion

In this thesis we have investigated the filament motions in magnetized plasmas in the Scarp-Off Layer. Using the continuity equation and coupling it with the compression of the electric currents we have provided a clear derivation of the two-field model equations that describe the evolution of the plasma density and vorticity. By linearizing the model equations we have derived the energy theorem for small density oscillations. This theorem yields that the sum of the kinetic and potential energy is a conserved quantity. This theorem has also showed that the filament structure is driven by the effective gravity through the particle flux. We have also derived the velocity scaling laws and shown that velocity scaling depends on the density oscillation amplitude. For small amplitudes velocity scales as a quadratic root of the amplitude, for large amplitudes velocity scales as unity.
Further, assuming non-isothermal electrons, we have derived the electron temperature equation for interchange motions from the energy equation and used this result to extend two-field model to the three-field model. In the isothermal limit this model reduces to two-field model equation described above. We have also derived an energy theorem considering small density and temperature oscillations and extending the definitions of the kinetic and the potential energy and showed that the temperature has the same contribution to the interchange motions as density. We have also found that it is possible to derive a velocity scaling law for the limit when amplitudes of the density oscillations are much larger than the amplitudes of the temperature oscillations. In this case velocity scaling for isothermal electrons is valid. When the amplitudes of the temperature oscillations are much larger that the amplitudes of the density oscillations,

velocity scales as a square root of the temperature amplitude, and this scaling is valid for all amplitudes.
We have verified the scaling laws numerically by solving the three-field model equations as diffusion-advection equations using spectral transformations. We have shown that the optimal results are provided when the domain length is 50, and the grid resolution is not less than 512×512. We have also found that the two-field model corresponds to the two-dimensional thermal convection on a thin fluid layer. We have showed that the maximum velocity becomes independent of the collisional dissipation for Ra$> 10^4$. These findings have allowed us to verify numerically all the velocity scaling laws that we derived in this thesis. All the theoretical expectations were met in the results of the numerical simulations.

Outlook and suggestions for the future work

As it was mentioned before, assumption about non-isothermal electrons is more natural, therefore the three-field model will help to understand more precisely the mechanisms of the filament motions in SOL-plasmas. This thesis may be considered as the first attempt to extend the existing and well-studied two-field model to the three-field model. We have in this study assumed that the density and the temperature have the same length scale. We can change this assumption and write model density and temperature as

$$\hat{n}(\hat{t} = 0) = 1 + \frac{\Delta n}{\mathcal{N}} \exp\left(-\frac{\mathbf{x}^2}{2l_{\hat{n}}^2}\right), \tag{4.1}$$

$$\hat{T}(\hat{t} = 0) = 1 + \frac{\Delta T}{\mathcal{T}} \exp\left(-\frac{\mathbf{x}^2}{2l_{\hat{T}}^2}\right), \tag{4.2}$$

where $l_{\hat{n}}$ denotes the characteristic length scale of the density, $l_{\hat{T}}$ denotes the characteristic length scale of the temperature, and perform systematic parameter study.
Another suggestion assumes a reconsideration of the polarization drift (2.32) that would let us derive the energy theorem for large oscillation amplitudes. We could also analogously to [18] investigate how temperature advection would affect entropy-like quantity and extend existing energy theorem.
Another suggestion offers inclusion of the sheath dissipation into the model and study of the effect from various sheath dissipation parameters analogously to [25]. In this case the vorticity equation would extend to

$$\frac{\partial \hat{\Omega}}{\partial \hat{t}} + \{\hat{\phi}, \hat{\Omega}\} + \hat{T}' \frac{\partial \hat{n}'}{\partial \hat{y}} + \frac{\partial \hat{T}'}{\partial \hat{y}} = \kappa \hat{\nabla}_{\perp}^2 \hat{\Omega} + \Lambda \hat{\phi}, \tag{4.3}$$

where Λ is a non-dimensional sheath dissipation coefficient.

Bibliography

[1] J Ongena et al. Energy for future centuries - Will fusion be an inexhaustible, safe and clean energy source?. *Fusion Science and Technology*, 45(2T):9–11, 2001.

[2] M. Taube and W. Seifritz. The search for a strategy for mankind to survive the solar Red Giant catastrophe. *ArXiv e-prints*, November 2008.

[3] K. Lackner et al. Fusion Physics,International Atomic Energy Agency, Vienna, 7 2012.

[4] M. J. FORREST P. D. WILCOCK V. V. SANNIKOV N. J. PEACOCK, D. C. ROBINSON. Measurement of the electron temperature by thomson scattering in tokamak t-3. *Nature*, 224(8):488–490, 1969.

[5] S.I. Krasheninnikov. On scrape off layer plasma transport. *Physics Letters A*, 283(5):368 – 370, 2001.

[6] D. P. Stotler S. J. Zweben, J. L. Terry and R. J. Maqueda. Invited review article: Gas puff imaging diagnostics of edge plasma turbulence in magnetic fusion devices. *Review of Scientific Instruments*, 3(88):2020–2026, 7 2003.

[7] Ralph Kube. Numerical studies of radial filament motion in toroidally confined plasmas. Master's thesis, University of Tromsø, May 2010.

[8] Ralph Kube. *Dynamics and statistical properties of blob structures in scrape-off layer plasmas*. PhD thesis, Faculcy of Science and Technology, Departament of Physics, 2014.

[9] Odd Erik Garcia. Plasma fluid models i, 2016. Lecture notes in FYS-3026 Fusion plasma physics.

[10] Odd Erik Garcia. Magnetohydrodynamics, 2016. Lecture notes in FYS-3026 Fusion plasma physics.

[11] Kerson Huang. *Statistical Mechanics*. New York: Wiley, 2 edition, 1987. p. 52-53.

[12] J. A. Bittencourt. *Fundamentals of Plasma Physics*. Springer-Verlag New York, 3 edition, 2004.

[13] Odd Erik Garcia. Guiding center motions, 2015. Lecture notes in FYS-2009 Introduction to Plasma Physics.

[14] Francis F. Chen. *Introduction to plasma physics and controlled fusion*, volume 1 of *2*. Springer Science+Business Media New York, 1984. p. 204.

[15] O. E. Garcia, N. H. Bian, and W. Fundamenski. Radial interchange motions of plasma filaments. *Physics of Plasmas*, 13(8):082309, 2006.

[16] D. A. Russell, D. A. D'Ippolito, and J. R. Myra. On relaxing the Boussinesq approximation in scrape-off layer turbulence (SOLT) model simulations. In *APS Meeting Abstracts*, October 2012.

[17] Odd Erik Garcia. *Convection and shear flows in fluids and magnetized plasmas*. PhD thesis, Faculcy of Science and Technology, Departament of Physics, 2002.

[18] R. Kube, O. E. Garcia, and M. Wiesenberger. Amplitude and size scaling for interchange motions of plasma filaments. *Physics of Plasmas*, 23(12):122302, 2016.

[19] O. E. Garcia, V. Naulin, A. H. Nielsen, and J. Juul Rasmussen. Turbulence and intermittent transport at the boundary of magnetized plasmas. *Physics of Plasmas*, 12(6):062309, 2005.

[20] Odd Erik Garcia. Plasma fluid models ii, 2016. Lecture notes in FYS-3026 Fusion plasma physics.

[21] Erich Zauderer. *Partial Differential Equations of Applied Mathematics*. John Wiley and Sons, Inc, 2006.

[22] Matteo Frigo and Steven G. Johnson. The design and implementation of fftw3. In *PROCEEDINGS OF THE IEEE*, pages 216–231, 2005.

[23] G Decristoforo R Kube, O E Garcia. Github - two-dimensional diffusion-advection solver. `https://github.com/rkube/2dads`, 2017.

[24] Gregor Decristoforo. Numerical computations of turbulent motions in

magnetized plasmas. Master's thesis, UiT The Arctic University of Norway, Faculcy of Science and Technology, Departament of Physics, May 2016.

[25] R. Kube and O. E. Garcia. Velocity scaling for filament motion in scrape-off layer plasmas. *Physics of Plasmas*, 18(10):102314, 2011.